GRAVITY+: Towards Faint Science, All Sky, High Contrast, Milli-Arcsecond Optical Interferometric Imaging

White Paper and Proposal

For the GRAVITY+ Consortium (MPE, LESIA, IPAG, UoC, CENTRA, MPIA, UoS):

F. Eisenhauer[1] (PI), P. Garcia[2,3,4] (CoI), R. Genzel[1,5], S. Hönig[6] (CoI[*]), L. Kreidberg[7,8] (CoI), J.-B. Le Bouquin[9] (CoI), P. Léna[10], T. Paumard[10] (CoI), C. Straubmeier[11] (CoI)

Senior Team Members and Associated Partners:

A. Amorim[2,12], W. Brandner[8], M. Carbillet[13], V. Cardoso[2,14], Y. Clénet[10], R. Davies[1], D. Defrère[15], T. de Zeeuw[1,16], G. Duvert[9], A. Eckart[11,17], S. Esposito[18], M. Fabricius[1,19], N.M. Förster Schreiber[1], P. Gandhi[6], E. Gendron[10], S. Gillessen[1], D. Gratadour[10], K.-H. Hofmann[17], M. Horrobin[11], M. Ireland[20], P. Kervella[10], S. Kraus[21], S. Lacour[10], O. Lai[22], B. Lopez[22], D. Lutz[1], F. Martinache[22], A. Meilland[22], F. Millour[22], T. Ott[1], R. Oudmaijer[23], F. Patru[10], K. Perraut[9], G. Perrin[10], R. Petrov[22], S. Quanz[24], S. Rabien[1], A. Riccardi[18], R. Saglia[1,19], J. Sánchez Bermúdez[8,25], D. Schertl[17], J. Schubert[1], F. Soulez[26], E. Sturm[1], L.J. Tacconi[1], M. Tallon[26], I. Tallon-Bosc[26], E. Thiébaut[26], F. Vidal[10], G. Weigelt[17], A. Ziad[13]

Supporters:

O. Absil[15], A. Alonso-Herrero[27], R. Bender[1,19], M. Benisty[9,28], J.-P. Berger[9], E. Banados[8], C. Boisson[29], J. Bouvier[9], P. Caselli[1], A. Cassan[30], B. Chazelas[31], A. Chiavassa[32], F. Combes[33], V. Coudé du Foresto[10], J. Dexter[1,34], C. Dougados[9], Th. Henning[8], T. Herbst[8], J. Kammerer[20], M. Kishimoto[35], L. Labadie[11], A.-M. Lagrange[9], A. Marconi[36], A. Matter[13], Z. Meliani[29], F. Ménard[9], J. Monnier[37], D. Mourard[13], H. Netzer[38], N. Neumayer[8], B. Peterson[39,40,41], P.-O. Petrucci[9], J.-U. Pott[8], H.W. Rix[8], D. Rouan[10], H. Sana[42], D. Segransan[31], H. Sol[29], E. van Dishoeck[1,16], F. Vincent[10], M. Volonteri[30], A. Zech[29]

(Affiliations can be found after the references)

---

[*] Conditional to funding approval

1   Executive Summary

GRAVITY and the VLTI have transformed optical interferometry with groundbreaking results on the Galactic Center, active galactic nuclei, and exoplanets.

The proposed upgrades of GRAVITY and the VLTI – in the following referred to as the GRAVITY+ upgrades – will open up the extragalactic sky for milli-arcsec resolution interferometric imaging, and give access to targets as faint as K = 22 mag. GRAVITY+ will measure the black hole masses of active galactic nuclei across cosmic time, and obtain high quality exoplanet spectra and orbits.

The estimated cost for the GRAVITY+ upgrades with wide-field off-axis fringe tracking, improved sensitivity, and laser guide star adaptive optics is relatively modest, and for the adaptive optics, renders unnecessary a separate obsolescence program for the current adaptive optics MACAO. The GRAVITY+ consortium is prepared to cover 70 % of the hardware cost, and to provide all personnel for those GRAVITY+ work packages that can efficiently be executed outside of ESO.

The GRAVITY+ upgrades can start immediately, and can be implemented incrementally, keeping the impact on operation to a minimum. They will add new, worldwide unique, science capabilities with every step. As an infrastructure upgrade of the VLTI, GRAVITY+ will serve all present and future VLTI instruments along with their communities.

The consortium is prepared and has the resources in hand to start the first upgrades immediately.

2 Introduction and Overview

Ever since the development of 'aperture synthesis' spatial interferometry at radio wavelengths in the 1950s (Jennison 1958, Ryle & Hewish 1960), this technique has been the standard choice for the development of large aperture, high angular resolution telescopes in the microwave and radio bands (Thompson, Moran & Swenson 2017).

Why has this not been the case in infrared and optical astronomy?

The principle of radio interferometry is based on measuring the complex mutual visibility of a celestial source on a number of baselines, each with two antennas, and then as a function of the baseline length and orientation in the u-v plane on the sky. For optimum operation, each telescope must be single-moded (diffraction-limited), with a flat wavefront across its aperture. With low-noise, phase-sensitive radio frequency band, or down-converted intermediate frequency band amplifiers on each telescope, all $N·(N-1)/2$ baselines of an N-telescope array can be measured simultaneously with little loss of signal or additional extra noise, in that way allowing efficient coverage of many u-v combinations on the sky. The source brightness distribution is the Fourier Transform of the complex visibility distribution in the u-v plane, and hence the u-v sampling determines the effective point spread function ('dirty beam') of the interferometer. Since early radio interferometry operated with moderately narrow bandwidths $\Delta\lambda$, the 'delay' coherence length of the 'fringe' is large, $\Delta l » \lambda/20 · (\lambda/\Delta\lambda)$. Also the atmospheric coherence length, the Fried parameter $r_0(\lambda)$ (Beckers 1993), and the associated coherence time $\tau_{atm} » r_0/v_{wind}$, are large at radio wavelengths (e.g., $r_0 » 2$ km and $\tau_{atm} » 1$ minute for $\lambda » 1$ cm). As a result, the coherence over the optical path length difference (OPD) on a given baseline can be maintained fairly easily and a large isoplanatic angle allows phase-referencing sources over a wide field-of-view.

The situation in the optical and infrared is very different. Because of the short wavelengths, the product of 'delay' coherence length and atmospheric coherence time and length is $» 10^5...10^8$ smaller than in the microwave-radio bands. In addition, optical interferometers require multi-mirror, free beam propagation, which results in much lower throughputs than in the radio. On the other hand, flux densities in the Rayleigh-Jeans limit scale as T/λ^2 such that for thermal sources ($T » 10^{2...4}$ K), the shorter wavelengths enjoy a corresponding advantage. Starting with the first attempts of stellar interferometry by Michelson & Pease (1921), the historical evolution of optical interferometry has been slow, primarily because of the difficulty of controlling the OPD. One way to beat the OPD control problem is to use narrow-band, heterodyne techniques also in the mid-infrared (Johnson, Betz & Townes 1974), albeit at a huge cost in sensitivity due to quantum noise and narrow-band operation[1].

Next, since the Fried parameter for good atmospheric conditions $r_0 = 15$ cm x $(\lambda/0.5\ \mu m)^{6/5}$ (Beckers 1993) is much smaller than the mirror diameter D for large ground-based telescopes, the wavefront over the telescope primary aperture is not flat. As a result, most dedicated optical/infrared interferometers have employed small telescopes (e.g., Shao et al. 1988).

---

[1] The narrow-band limitation for heterodyne interferometry could in principle be overcome by multiplexing, but this technique is still in a very early stage of development for optical interferometry.

Therefore scientific applications have been limited to 'bright' stellar science and a few bright extragalactic targets (e.g., Quirrenbach 2001, Jaffe et al. 2004, Weigelt et al. 2012).

These challenges were anticipated in the design of the VLTI by preferring infrared over visible wavelengths and by co-phasing the 8 m telescopes with adaptive optics (Léna 1979, Woolf & Angel 1981).

Finally, there are no low-noise heterodyne mixers and amplifiers, and complex visibilities are measured in direct detection, typically with wide bandwidths. This means that for multiple aperture interferometry the incoming beams have to be split to form the $N \acute{} (N-1)/2$ baselines, resulting in large light losses per beam.

Taken together it is clear that infrared/optical interferometry is orders of magnitude more challenging than radio interferometry.

How can one then get to 'faint' science applications, and to larger sky coverage of extragalactic targets?

2.1   GRAVITY: the Keys to Success

The GRAVITY interferometric beam combiner at the VLT was designed and developed primarily for overcoming several of the above technical difficulties and hence for facilitating faint-target science (GRAVITY Collaboration et al. 2017a), with the following key features,

1. the first key step towards faint-target science interferometry in GRAVITY is to include the 8 m telescopes for sensitivity, and equip each of the four UTs with infrared wavefront sensors, adaptive optics systems (CIAO, Scheithauer et al. 2016), as already envisioned in the original design strategies for the ESO-VLTI (Léna & Merkle 1989);

2. the second breakthrough was the implementation of robust fringe tracking to make possible minute-long science exposures (Lacour et al. 2019). One key to success was to operate in the astronomical K-band, which is better matched to the current adaptive optics performance and vibration background of the UT telescopes;

3. for both adaptive optics correction and fringe tracking, the measurement has to occur at kHz rates and read noise has to be minimized. For this purpose the SAPHIRA-SELEX system was developed (Finger et al. 2016), which is a HgCdTe 320 x 256 $pixel^2$, electronic avalanche photo diode, imaging detector with effective read noise of 1.3 e^- at 300 – 1000 Hz;

4. to avoid bulky, warm optics and to realize an efficient throughput (34%), GRAVITY does the beam extraction, combination, manipulation and detection in a cryogenic environment (the 'Beam Combiner Instrument'), and with single-mode, super-balanced fluoride glass fibers. The fibers also act as spatial filters to reject non-coherent light and to improve fringe detection and tracking, as well as visibility calibration. Variable mechanical stretching of the $\gg$ 16 m fiber spools is used for differential delay line compensation and achieving nm-precision in feed-back loop operation with the fringe tracker and the GRAVITY laser metrology system. The GRAVITY fiber coupler (Pfuhl et al. 2014) is designed to send the light of one (self-

fringe tracking) or two (phase-referenced fringe tracking) objects in the focal plane to one or two fibers per telescope;

5. GRAVITY combines the telescope beams of all four UTs in an integrated optics, silica chip manufactured by CEA/LETI (Jocou et al. 2014, Perraut et al. 2018), which efficiently splits the light into the six baselines, and instantaneously samples the fringes in four delays, such that the on-fringe OPD can be efficiently detected without scanning. There are two beam combiners, one for the fringe tracker, and one for the second science object;

6. GRAVITY includes two cryogenic spectrometers (Straubmeier et al. 2014) for the 1.95 – 2.45 µm (K-band) range. Each spectrometer is fed by the 24 outputs of the integrated optics beam combiners. One disperses each output into six spectral pixels for low noise, fast fringe tracking; the second (science) spectrometer is optimized for second to minute integrations at selectable spectral resolving powers of 22, 500 and 4500. The spectrometers can be operated with or without a Wollaston prism to split the linear polarizations of the light;

7. the GRAVITY metrology (Lippa et al. 2016) measures the differential optical path between the two stars in the VLTI beam relay (all the way to the UT primary mirror) and the Beam Combiner Instrument. This scheme has the advantage of being largely insensitive to vibrations in the VLTI optical train;

8. GRAVITY includes a highly sophisticated control system, including wavefront and pupil control at the telescope and instrument level, optical path length control for fringe tracking and astrometry, metrology-based fiber control, vibration compensation as part of the adaptive optics and fringe tracking;

9. a final element of the GRAVITY development has been the continuing optimization and consistent upgrading of operational efficiency since the first commissioning of the instrument on Paranal in late 2015, such that high-quality interferometric imaging, imaging spectroscopy, and polarimetry data can be routinely obtained under good conditions. The outstanding and wholehearted support by the Paranal staff was and is an important element of this continuing progress.

2.2 Performance Increase by Large Factors

The resulting performance has arguably transformed optical interferometry. Before GRAVITY, the limiting magnitude for near-infrared interferometry was typically around K $\gg$ 6 – 10 mag, with a one-time record of K = 12.5 mag for a technical observation (Woillez et al. 2014).

In single-object tracking (self-referenced) mode, GRAVITY now routinely does interferometric broadband and spectroscopic imaging at K $\gg$ 11 mag. For bright objects, GRAVITY has measured visibilities to an accuracy better than 0.25 %.

In dual-object, externally fringe tracking mode, GRAVITY has already achieved or outperformed its original design specifications of achieving K = 17 mag milli-arcsec imaging, and 10 – 30 micro-arcsec astrometry at K = 15 mag (Eisenhauer et al. 2008). The background in the deepest GRAVITY images of the Galactic Center in 2018 combining several nights has an rms noise better K = 21 mag (several thousand times deeper than previous observations). The astrometric observation of a bright SgrA* flare in July 2018 (GRAVITY collaboration et al.

2018b) has astrometric uncertainties of ±20 micro-arcsec, more than 20 times better than previous astrometry with adaptive optics using a single telescope. GRAVITY also has successfully demonstrated percent-level polarimetric measurements, and differential spectral astrometry at the level of 0.06 degrees rms in interferometer phase (or < 1 micro-arcsec on sky, GRAVITY collaboration et al. 2018d).

GRAVITY is also the first interferometer to routinely offer dual-field astrometry for faint objects. Searching for the astrometric signatures of exoplanets, GRAVITY monitoring of the 2 arcsec separation M-star binary GJ65 measures the relative position of the stars to a level of 3×10^{-5}. In the first detection of a planet by optical interferometry, GRAVITY has achieved a contrast of 11 mag between the planet HR8799e and its host star at 390 milli-arcsec separation (GRAVITY collaboration et al. 2019b). Here, another well-known advantage of interferometry comes to the fore, namely the elimination of atmospheric antenna-based noise. The optical / infrared equivalent is residual speckle noise, which cannot be effectively suppressed in adaptive optics assisted telescope observations using a coronograph. GRAVITY filters out this fundamental noise.

2.3   The Harvest of the First Three Years

GRAVITY has already provided groundbreaking results covering a broad range of astrophysical science (Figure 1):

- GRAVITY has delivered precision tests of Einstein's general theory of relativity and the so far strongest experimental evidence that the compact mass in the Galactic Center (SgrA*) is indeed a Schwarzschild-Kerr black hole (GRAVITY Collaboration et al. 2018a,b, 2019a, 2020c, Figure 1 top right, and center, Figure 2);
- GRAVITY has delivered a 0.33 % accuracy direct determination of the distance between the Sun and the Galactic Center (GRAVITY Collaboration et al. 2019c);
- GRAVITY has revealed that the ionized gas in the broad line region (BLR) of the type 1 quasar 3C 273 is comprised of an » 0.1 parsec (pc) turbulent rotating disk and has determined the mass of the central black hole with an error of 40 % (GRAVITY Collaboration et al. 2018d, Figure 1 top middle). A large program, started on the VLTI in 2019, aims at increasing the statistics of such directly determined black hole masses, which will yield an absolute calibration of the empirical, black hole mass-luminosity relation inferred from reverberation mapping of active galactic nuclei (AGN);
- GRAVITY has mapped the hottest dust in the nearby type 2 Seyfert galaxy NGC 1068 and unveiled a disk of about 1 pc diameter associated with the H_2O masers. GRAVITY finds that this disk is not a thick torus, as postulated by the standard 'unified scheme' for AGN (GRAVITY Collaboration et al. 2020a, Figure 1 top left);
- GRAVITY has provided clear evidence that the majority of the massive stars in the Orion Trapezium region are multiple (GRAVITY Collaboration et al. 2018e, Figure 1 bottom left);
- GRAVITY has yielded milli-arcsec imaging spectroscopy of the gas in η Car and jet in SS433 with remarkable detail and complexity (GRAVITY Collaboration et al. 2017b, 2018c, Waisberg et al. 2019, Figure 1 bottom right);

- GRAVITY has obtained the first high spectral resolution, interferometric observations of a classical T Tauri star, resolving the HII region of the S CrA binary (GRAVITY Collaboration et al. 2017c). Recent observations have for the first time spatially resolved the magnetospheric accretion in young Sun-like stars (GRAVITY collaboration et al. 2020d, Bouvier et al. 2020).
- GRAVITY has resolved, for the first time, the two images generated by a gravitational microlens (Dong et al. 2019, Figure 1 bottom middle), and in combination with SPITZER space telescope data measured the lens mass of a nearby microlensing event (Zang et al. 2019);
- GRAVITY has provided outstanding, high-quality atmospheric spectra of two young hot Jupiter exoplanets, ten times better than previous coronographic integral field spectroscopy (GRAVITY Collaboration et al. 2019b, 2020b, Figure 1, bottom second from right). A large program has just started, and its first observations have already measured ten exoplanets, including the first direct detection of an exoplanet initially discovered by the radial velocity method, ß Pic c.
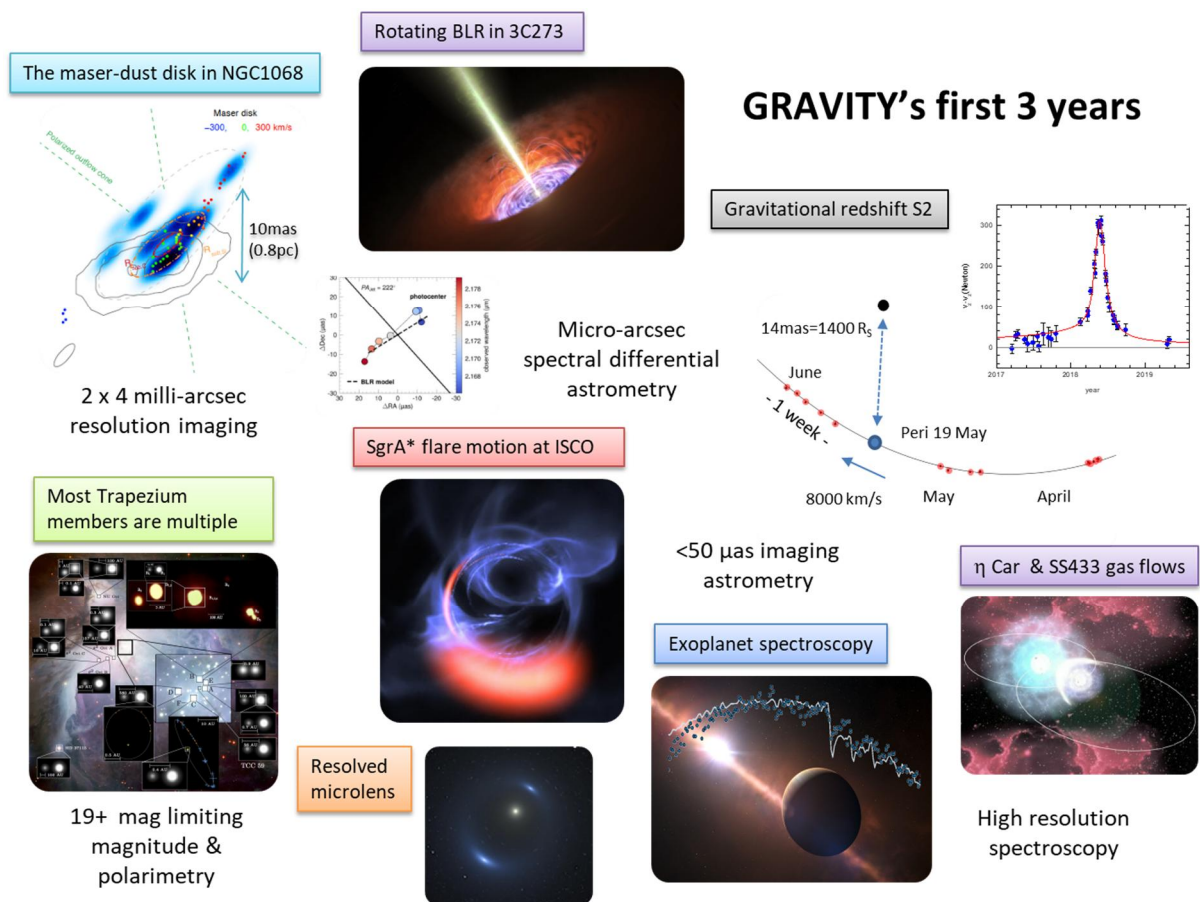
Figure 1. Summary of the scientific results from the first three years of GRAVITY (2017 – 2019). This slide summarizes the remarkable depth and range of astronomy demonstrated with this new instrument, from exoplanets, circumstellar gas and dust, X-ray binaries, stellar black holes, and microlenses, to the detailed kinematics near the massive black hole in the Galactic Center, and then out to the circumnuclear and broad-line regions around active galactic nuclei.

2.4   Inward Bound: Testing the Massive Black Hole Paradigm

As a more detailed example of the progress that has become possible, Figure 2 summarizes the progress in the empirical determination of the Galactic Center mass distribution since the mid-80s, at which time measurements of the Doppler velocities of ionized and neutral gas clouds around SgrA* for the first time indicated the presence of a spatially concentrated central mass. With the MPE high resolution stellar orbit (especially the star S2) monitoring program at ESO starting in 1991, and that of Ghez et al. at the Keck telescope in 1995, there is now a convincing case that this concentration of 4.1 million solar masses is coincident with the compact radio source SgrA*. With the detections of gas motions near the innermost stable circular orbit, this mass must be concentrated within 7 – 10 gravitational radii R_g of a 4 million $M_\odot$ Schwarzschild-Kerr black hole. By resolving the sphere of influence of the central mass over six orders of magnitude in spatial scale, the Galactic Center provides by far the best case for the existence of massive black holes (MBHs) as predicted by General Relativity, although more speculative configurations, such as massive boson stars or gravastars, cannot yet be unequivocally excluded. In a broader comparison, the 'Kerr-ness' of SgrA* is now confirmed to a level of rigor on par with the 30 $M_\odot$ stellar black holes by aLIGO.

While the compact mass associated with SgrA* is located in a very dense star cluster, including the enigmatic S-stars, which probably have been captured from binaries by the central object during their flyby on near loss-cone orbits, the extended mass within the S2 orbit is < 0.2 % of the central mass. In terms of other tests of General Relativity near a SMBH, the GRAVITY collaboration (2020c, in prep.) expects to report on the detection of the Schwarzschild precession of the S2 orbit later this year.

3 Science Cases for GRAVITY+

The above examples give a first glimpse of what optical/infrared interferometry on 100m+ baselines is capable of when it is sensitive enough to track the fringes on faint stars. GRAVITY now allows milli-arcsec interferometric imaging and micro-arcsec differential spectroscopic astrometry for tens of external galaxies out to a redshift z < 0.2. Perhaps the most important next question is whether it is possible, and what it would take, to expand interferometric capabilities still further, towards K > 22 mag, all-sky extragalactic observations for a large community of users. In line with ESO's 'VLTI roadmap' (Mérand 2018), the proposing team has started to investigate the possibilities and priorities for further upgrading the capabilities and sensitivity of GRAVITY and the VLTI. The following sections discuss several key science cases that will be enabled with GRAVITY+.

3.1 The Galactic Center

The goals of future Galactic Center observations with GRAVITY+ are threefold.

The first is on faint stars near SgrA* for determining the spin of the MBH. Waisberg et al. (2018) have analyzed in detail how precision astrometry of such a K > 19 mag star can be used to achieve this fundamental goal for testing the massive-black hole paradigm. GRAVITY recently detected a K $\gg$ 19 mag star near SgrA*, inside the S2 orbit, and its properties are currently analyzed. Measurements of the spin magnitude and direction in the Galactic Center are fundamental for physics and astronomy. The magnitude of the spin gives interesting insights on the average 'feeding pattern' of a MBH in an equilibrium, star forming, main-sequence disk galaxy. Its direction will give information on the source of the current, low-level gas accretion, likely connected to stellar winds of massive stars in a thick, clockwise disk on $\gg$ 0.1 pc scale (GRAVITY Collaboration 2018b).

With the improved sensitivity and Strehl ratio of GRAVITY+, studies of the stellar and gravitational environment close to SgrA* will become more sensitive, and present the second goal in the Galactic Center. Several to some tens of stars and stellar black holes are expected in this central zone from numerical simulations (Figure 2, left panel). They give important information on extreme mass ratio in-spiral rates into MBHs, of fundamental importance for the LISA gravitational wave mission. The available GRAVITY data already strongly exclude the presence of a second, intermediate mass black hole > 10^3 M$_\odot$ near SgrA* (Figure 2, right).

Perhaps the most exciting, third goal will be the study of the magnetic field structure and hot gas motions near the innermost stable orbit. With GRAVITY+ astrometric precision of 10 – 30 micro-arcsec, studies of flare motions and polarization will vastly improve the quality and quantity of flares that can be studied in this way and give a much-improved view of the gas dynamics in the innermost accretion zone around a MBH.
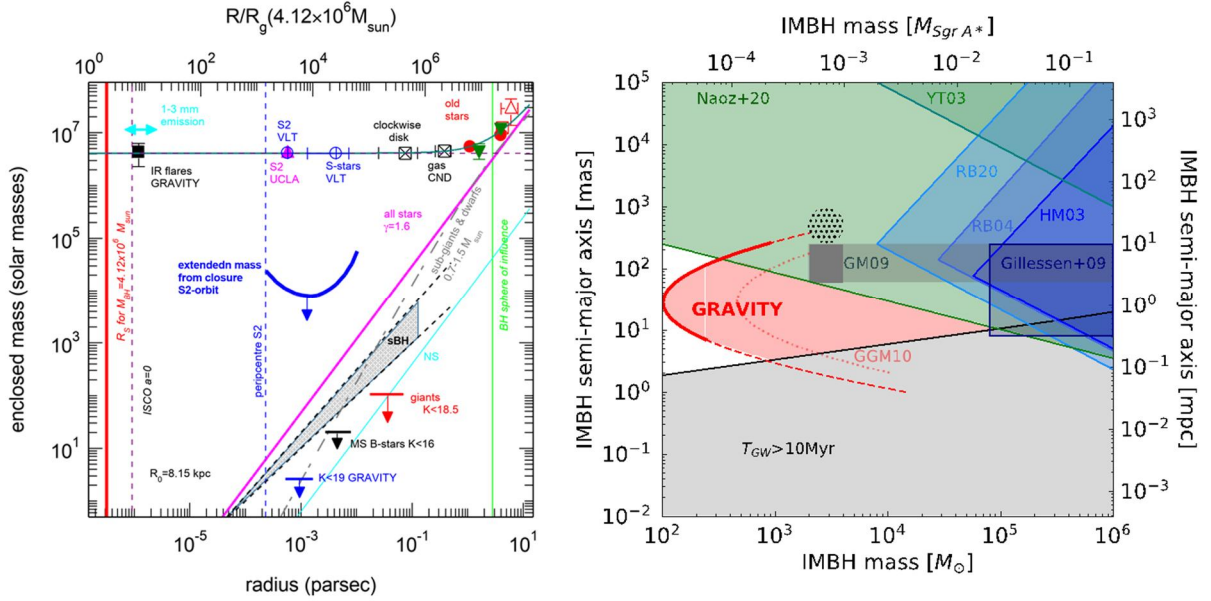
Figure 2. Constraints on the extended mass (left) and the eventual presence of a second, intermediate mass black hole (IMBH) in the Galactic Centre (right). Left: enclosed mass in the central 10 pc of the Galaxy (see GRAVITY Collaboration 2018a,b, 2019c, 2020c). The blue crossed circle, the pink triangle, and the black crossed rectangles are estimates of the enclosed mass within the S2-orbit, other S-stars and the massive star disks. The measurements at larger separation are from late-type stars and the rotating gas in the circumnuclear disk (see Genzel, Eisenhauer & Gillessen 2010 for details). The filled black rectangle comes from the clockwise loop-motions of near-IR flares (GRAVITY Collaboration 2018b). The cyan double arrow denotes current VLBI estimates of the 3 mm size of SgrA*. The diagonal lines show the total mass from all stars and stellar remnants, sub-giants, and dwarfs. The grey-hatched conus indicates the distribution of stellar black holes and neutron stars from simulations of Baumgardt, Amaro-Seoane & Schödel (2018). Red, black and blue upper limits denote upper limits on giants, main-sequence B-stars and K < 19 GRAVITY sources. Red and grey dotted vertical lines give the Schwarzschild radius of a $4 \times 10^6 M_\odot$ black hole and the innermost stable circular orbit radius for a non-spinning black hole. The pericentre radius of S2 is the dotted vertical blue line. The convex blue curve denotes the 2σ upper limit of any extended mass around SgrA* obtained from the lack of retrograde precession in the S2 orbit. Right: Limits on a second IMBH as a function of its mass and separation from SgrA*. The shaded area is excluded observationally. Adapted from Gualandris & Merritt (2009). The blue regions are excluded because of the stationarity of the radio source SgrA*, the bottom area would lead to a gravitational wave inspiral in $< 10^7$ years. GRAVITY and the lack of extra residuals in the orbit of S2 exclude the red-shaded region. All but a $10^2 - 10^3 M_\odot$ IMBH inside the orbit of S2 or just outside of S2's orbit is now excluded by the various measurements.

3.2 The Cosmic Evolution Explorer – Active Galactic Nuclei at Low and High z

3.2.1 The Galaxy/AGN Co-Evolution and Super Massive Black Hole Masses

Essentially all massive galaxies in the universe host a supermassive black hole (SMBH) in their centre with masses in the range of about 10^6 to 10^{10} $M_\odot$. Curiously, the mass of the black holes are tightly correlated with properties of the host galaxy, with the most prominent ones being the correlation of black hole mass and stellar velocity dispersion, and the bulge stellar mass. On the other hand, the supermassive black hole contributes only a small fraction of typically $\gg 0.1$ % to the mass of the central galaxy, so why should the galaxy care about the black hole?

Physical processes at play during early stages of galaxy formation provide important clues into why galaxies and SMBHs co-evolve. However, essentially all our current knowledge of the evolution of supermassive black holes relies on scaling relations that have been derived locally (redshift z < 0.3) via AGN reverberation. Moreover, the typical SMBH mass range of active galactic nuclei (AGN) and quasars (QSOs) probed with reverberation mapping is rather narrow, typically $10^{7...8}$ $M_\odot$. These local relations are then applied to SMBHs at much higher redshift and for higher masses ($10^{9...10}$ $M_\odot$), where reverberation mapping campaigns require continuous multi-year to decade-long monitoring to reliably recover the emission line lags as both the dynamical time scales ($\propto M_{BH}$) and cosmological time dilation ($\propto (1+z)$) increase the lags. This severely limits our understanding of galaxy/SMBH co-evolution and of the high redshift population of SMBHs in general.

GRAVITY+ opens the opportunity to directly map the galaxy/SMBH co-evolution through the peak of cosmic galaxy growth by dynamically measuring the SMBH masses from low to high redshift, independent of the reverberation technique. While a few local SMBHs are in reach with the current instrument, the significantly improved sensitivity of GRAVITY+ will make it a true cosmic evolution explorer. Figure 3 gives a first assessment of the increase in AGN samples, facilitated by the GRAVITY+ upgrades, which demonstrates that the number of accessible type 1 AGN increases dramatically, to hundreds for z < 0.3, $\gg 100$ at z $\gg 0.8 - 1$, and a good dozen QSOs at z $\gg 2$. With 30″ external fringe tracking, the number of z $\gg 2$ targets increases still further to $\gg 100$. This includes a number of compact binary radio AGN. These samples probe into the peak of cosmological black hole growth and star formation (Figure 4), hence spatially resolving the dynamical processes in sources where co-evolution is strongest.

3.2.2 Super-Eddington Accretion

Today more than 100 QSOs at z>6 are known (Banados et al. 2016). These SMBHs must have been growing at the most efficient rate in order to appear so early in the history of the Universe. Super-Eddington accretion on to massive black hole seeds may play an important role and be commonplace in the early Universe (e.g., Regan et al. 2009). Indeed, cases with ratio of bolometric and Eddington luminosity $L_{bol}/L_{edd} > 9$ have been suggested at high redshift (e.g., Tang et al. 2019). However, such claims are based on black hole mass estimates derived from the local $R_{BLR} - L_{AGN}$ scaling relation, assuming the calibration in the local Universe is independent of redshift.
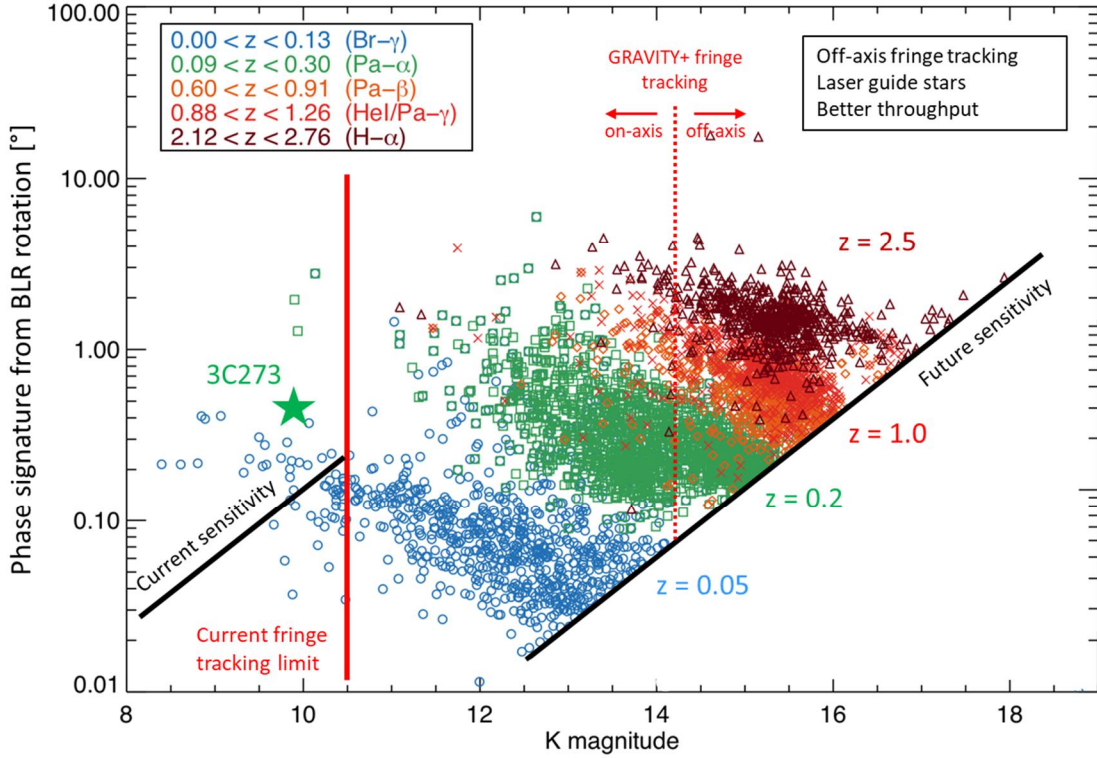
Figure 3. Impact of the increased sensitivity of GRAVITY+ on the number of type 1 QSOs, for which GRAVITY+ will spatially resolve their broad line region (BLR). There are about 20 BLR AGN detectable at the current sensitivity and on-axis fringe tracking limit. With the GRAVITY+ upgrades the number of AGN accessible with on-axis tracking increases dramatically, to hundreds of z < 0.3, » 100 at z » 0.8 – 1, and a good dozen z » 2 QSOs. With 30″ off-axis fringe tracking the number of z » 2 targets increases to » 100.
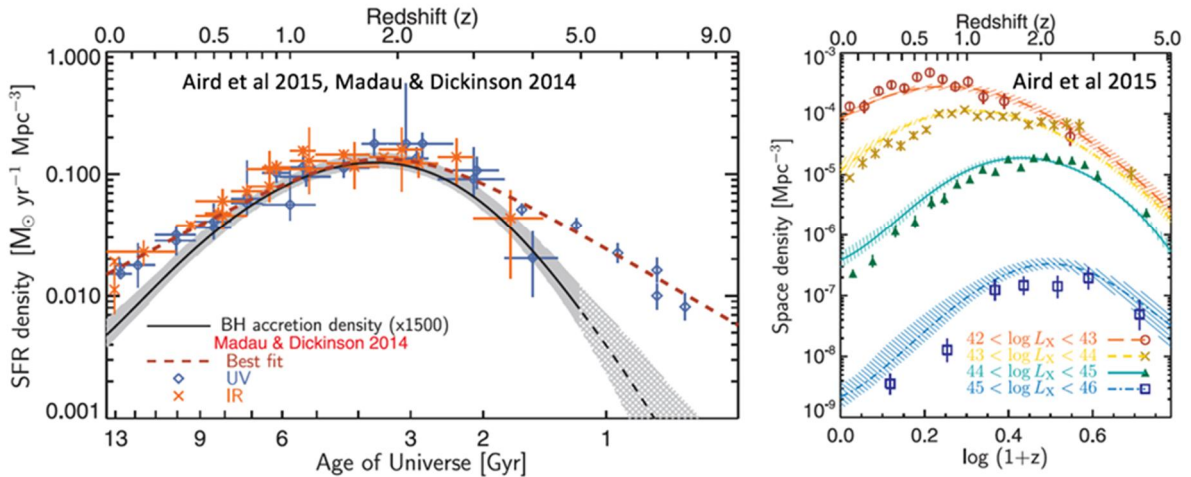

Figure 4. Left: Cosmic star formation and black hole accretion history as function of redshift. Right: Space density of massive black holes (MBHs) of different X-ray luminosities. At redshift z » 2, GRAVITY+ will probe the peak of the black hole accretion history as well as the most luminous and active MBHs throughout cosmic time.

13

Super-Eddington accreting massive black holes in the local Universe usually have smaller BLRs than AGN with the same luminosities (Du et al. 2018). Spectro-astrometry with GRAVITY+ will extend size measurements and, combined with reverberation mapping, study physics of the super-Eddington accretion processes (e.g., self-shadowing effects in slim disks, Wang et al. 2014).

3.2.3   Tidal Disruption Events

Stars approaching too close to $< 10^8 M_\odot$ SMBHs are torn apart by tidal forces outside the event horizon. Some of the stellar debris is flung outward at high speeds, while the rest becomes hotter as it falls toward the black hole, causing a spectacular flare of electromagnetic radiation. Such tidal eruption events (TDE) could play an important role in the growth of SMBHs, probe relativistic effects of matter under strong gravity, probe super-Eddington accretion physics near the last stable orbit, and provide a new means of measuring black hole spin (the rates and light curves of tidal disruption events depend on MBH spins). They represent signposts of intermediate-mass MBHs, binary MBHs and recoiling MBHs in active and in-active galaxies (e.g., Komossa 2015, Leloudas et al. 2016).

The bright extreme UV and X-ray continuum of a TDE is reprocessed into emission lines by the surrounding nuclear gas. This emission line signal can be used for GRAVITY+ imaging or spectro-astrometry, analogously to the Broad Line Region region. Upcoming and longer-term future sky surveys predict to find TDEs in the hundreds to thousands, including in the radio with SKA, in the optical with LSST and in soft and hard X-rays with Einstein Probe and eRosita (e.g., van Velzen et al. 2011, Khabibullin et al. 2014). Many of these TDEs happen around SMBHs with masses of the order of $10^{6\ldots7} M_\odot$ at nearby redshifts of $z \approx 0.05\ldots0.1$, and will have a nearby star suitable for wide-field off-axis fringe tracking, permitting the first probe of the structure of the reprocessing gas. The GRAVITY+ schedule is well timed to make use of TDEs from these surveys given, for instance, the recent eROSITA launch and upcoming LSST.

3.2.4   The Last Parsec Problem – Binary Supermassive Black Holes

One of the consequences of merging galaxies is that their supermassive black holes should also merge. In a major binary galaxy merger (mass ratios $\approx$ unity) dynamical friction of the two supermassive black holes against the background galaxy merger should lead to a rapid in-spiral of the two black holes on a few times the orbital time scale ($\approx 10^{8.5}$ yr). This merging process is expected to stall at a separation of a few pc. This stalling radius is the sphere of influence of the black holes, at which dynamical friction ceases to be effective. Only at a separation below $\approx 10^{-3}$ pc, the emission of gravitational waves becomes effective in reducing the orbital separation. This is often referred to as the 'final parsec problem'. Deviations from circular symmetry in the nuclear gas distribution, or tri-axial stellar orbits may help to overcome the final parsec problem (e.g., Vasiliev, Antonini & Merrit 2015). However, the time scales involved of 10^8 to 10^9 years still imply that a significant fraction of supermassive black holes on parsec-scales should be binary (Begelman, Blandford & Rees 1980), while estimates range from 0.1 – 15 % for kiloparsec-scale binarity of the AGN population at redshifts $z \lesssim 1.5$ (Rosario et al. 2011, Solanes et al. 2019). Surprisingly, most observations suggest that supermassive black holes in the nuclei of local galaxies seem to be predominantly single. With the exception of VLBI techniques, no observations can directly probe the required scales, and

binary SMBH identification via double-peaked emission line profiles and dual jets/outflows remains ambiguous.

With GRAVITY+, it will be possible for the first time to probe radio-quiet parsec-scale binary SMBHs, from the local universe, through the 'peak of binarity' at z $\gg$ 0.6 – 1.3, and out to the cosmic peak of galaxy merging (z $\gg$ 2). GRAVITY+ can detect the tell-tale phase signatures of dual BLRs in close binary SMBHs (Songsheng et al. 2019). By providing spatial information, GRAVITY+ will be the ultimate instrument to firmly establish the binarity of candidates that are expected in the thousands from, e.g., upcoming surveys with SDSS-V and 4MOST. The infrared regime will overcome potential obscuration in these systems while removing the requirement for radio-loudness.

This GRAVITY+ science case is highly complementary to those of the $\gg$ 2035 LISA mission and pulsar timing array. This LISA space-based gravitational wave (GW) detector will be sensitive to mergers of supermassive black holes with separations $< 10^{-3}$ pc, both on an event-by-event basis as well as detection of a 'cosmic gravitational wave background'. Pulsar Timing Arrays operating in parallel will be able to predominantly pick up sources at smaller separations after crossing the parsec-scale barrier. GRAVITY+ will observationally narrow down the redshift range at which the expected GW signal peaks.

3.3   The Characterization of Exoplanets

The present-day atmospheric composition of exoplanets provides a fossil record of the planets' formation history and evolution (Madhusudhan 2019). However, despite intensive efforts to characterize the atmospheres of exoplanets with traditional techniques (transit spectroscopy and direct imaging), their chemical abundances are typically only known to about an order of magnitude (e.g., Kreidberg et al. 2014).

The unique observing capabilities of the GRAVITY instrument have already delivered measurements of exoplanet atmospheric compositions that are 50 – 100 x more precise than achieved before. For example, recent observations of the young extrasolar gas giant ß Pic b determined the carbon-to-oxygen ratio to 10 % (GRAVITY Collaboration et al. 2020b). Notably, this measurement is even more precise than that available for Jupiter (Li et al. 2020). To date GRAVITY has measured ten exoplanets (e.g., Eri b, HD95086b, HR8799bcde), including planets in protoplanetary disks, e.g., of PDS70. GRAVITY+ will peer deep into these regions of planet formation, and, e.g., probe the planetary nature of the radial velocity kinks seen with ALMA (Pinte et al. 2020).

Transit spectroscopy and spectroscopic imaging at its current sensitivity do not allow the characterization of mature, cold exoplanets. These planets are thought to form predominantly close to the ice-line (around 2 AUs, Fernandes et al. 2019). So far none has been directly imaged because of the high contrast to the host star: e.g., a Jupiter-like planet at 1 astronomical unit (AU) would be 10^7 times fainter than its host star, with an angular separation close to 100 milli-arcsec at a distance of 10 pc.
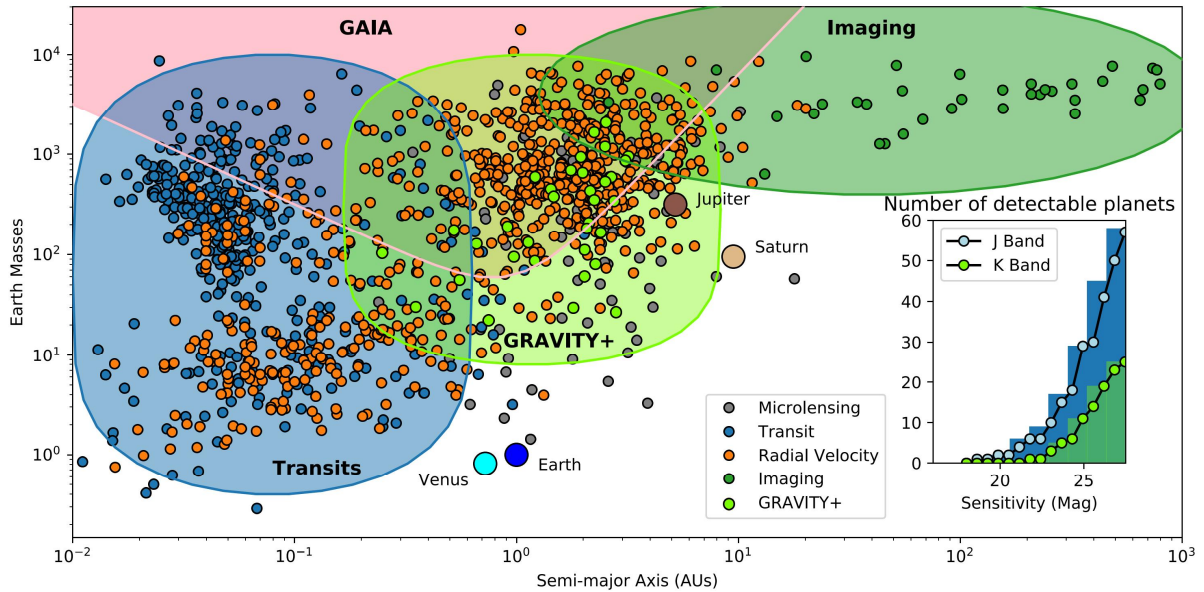
Figure 5: Known exoplanets from the NASA Exoplanet Archive. Over-plotted in light green are the planets that could be characterized with GRAVITY+ (assuming a distribution from Kopparapu et al. 2018). Inset: the number of detectable planets as a function of the sensitivity of GRAVITY+.

The proposed GRAVITY+ upgrades will enable the exploration of a sample of planets in a new part of parameter space — mature, cool exoplanets analogous to Jupiter.

These planets are inaccessible with current facilities: traditional direct imaging techniques do not have the sensitivity and contrast required to detect exo-Jupiters (which are 10^7 times fainter than their host stars, with angular separation of $\gg$ 100 mas). Jupiter analogs are also out of reach for transit spectroscopy, because their transits are infrequent and low-probability. GRAVITY+ will provide spectra for up to a dozen cold exoplanets in the K-band (Figure 5) to determine their chemical composition and cloud/haze properties, enabling comparative planetology with the Solar System. In addition, repeated observations have the potential to reveal weather – which is commonly seen in brown dwarfs, but never before in exoplanets (Radigan et al. 2012). The observation of the H_2O, CO, CO_2, CH_4, N_2O molecular bands in the K-band will allow the comparison with planets in our solar system, a step to address whether solar system planets are unusual in their chemical composition.

The high-order adaptive optics and enhanced vibration control from GRAVITY+ is also prerequisite for future visitor instruments outside the scope of GRAVITY+. For example, for on-axis nulling interferometry at L-band to study young Jupiter analogs within the snow line of nearby planet forming regions, and J-band observations, which could substantially increase the sample of Jupiter analogs, give access to the O_2 absorption bands, and will ultimately probe Earth-mass planets within the habitable zone around M-dwarfs, e.g., Proxima Cen b.

3.4 Young Suns and their Planet Forming Disks

Planets form a few million years after proto-stellar collapse, at an epoch when the young star still actively accretes from its circumstellar disk. The accretion of disk material onto the stellar surface directly impacts the star's properties and early evolution. It also produces high-energy radiation that illuminates the circumstellar disk and the proto-atmosphere of nascent planets, thus drastically changing their physical and chemical evolution. The star-disk interaction (e.g., Bouvier & Appenzeller 2008) takes place at a distance of few stellar radii, where the inner disk is magnetically truncated by the powerful stellar magnetosphere, and the material is forced to flow from the inner edge of the disk to the stellar surface along magnetospheric funnels (Figure 6).
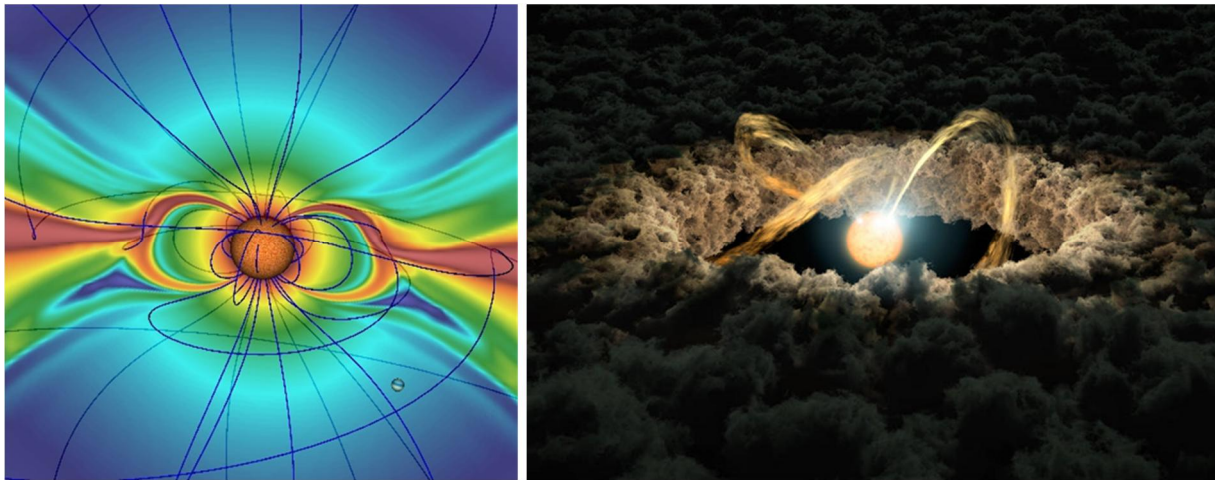

Figure 6. Computer simulations (left, spidi-eu.org) and artist impression (right, NASA/JPL-Caltech/R. Hurt(IPAC)) of magnetospheric accretion onto a forming star. The powerful stellar magnetosphere of the star truncates the inner disk, and the evaporating matter is funneled along magnetic field lines onto the star. GRAVITY+ will spatially and spectrally resolve several hundred such systems.

While current studies are mainly focused on intermediate-mass Herbig stars (Lazareff et al. 2017; GRAVITY Collaboration et al. 2019d), the improved sensitivity and sky coverage from GRAVITY+ opens up the observations of the dominant population of low-mass, young and embedded stars. These largely unexplored systems show magnetospheric accretion in a very different regime, with much higher accretion rates, stronger magnetic fields, and with probably much stronger impact on the inner part of the circumstellar disk. All young star-disk systems will undergo such an energetic period, while at the same time proto-planets are forming. GRAVITY+ will routinely detect differential astrometric signals in the spectral lines (e.g., HI Brg and CO lines) of the accreting and ejected gas at few tens of micro-arcsec resolution, corresponding to a few percent of an astronomical unit. A very strong synergy is expected with spectro-polarimeters monitoring the magnetic signatures (e.g., CFHT/SPIRou), and with MATISSE and ALMA, to provide a detailed picture all the way from the stellar surface to the outskirts of the planet-forming disks.

3.5 Microlenses

Interferometry offers a new revolutionary technique to characterize compact objects (brown dwarfs, white dwarfs, stellar black holes) through microlensing. A resolution of a few milli-arcseconds is necessary to resolve the lensed image. By measuring the Einstein radius of the lensed image (Einstein 1936), and in combination with the parallax and proper motions of the lensed source, one can directly and model-free determine the mass, distance and transverse velocity of the lens (i.e., the compact object). Interferometry has the advantage that already a single observation gives the Einstein radius. The last year has already seen the first two such measurements with GRAVITY (Dong et al. 2019, Zang et al. 2019, Figure 6 left). The performance and sky-coverage of GRAVITY+ will give access to thousands of microlenses predicted by Gaia (Bramich 2018) and/or detected by WFIRST and LSST (Sajadian & Radoslaw 2018). For events with long Einstein crossing times > 300 days, the chance that the lens is a stellar black hole is > 50 % (Lam et al. 2020, Figure 6 right). The follow-up observations with GRAVITY+, together with light curves and astrometry, will therefore allow measuring the stellar black hole mass function, their multiplicity, and kick velocity.
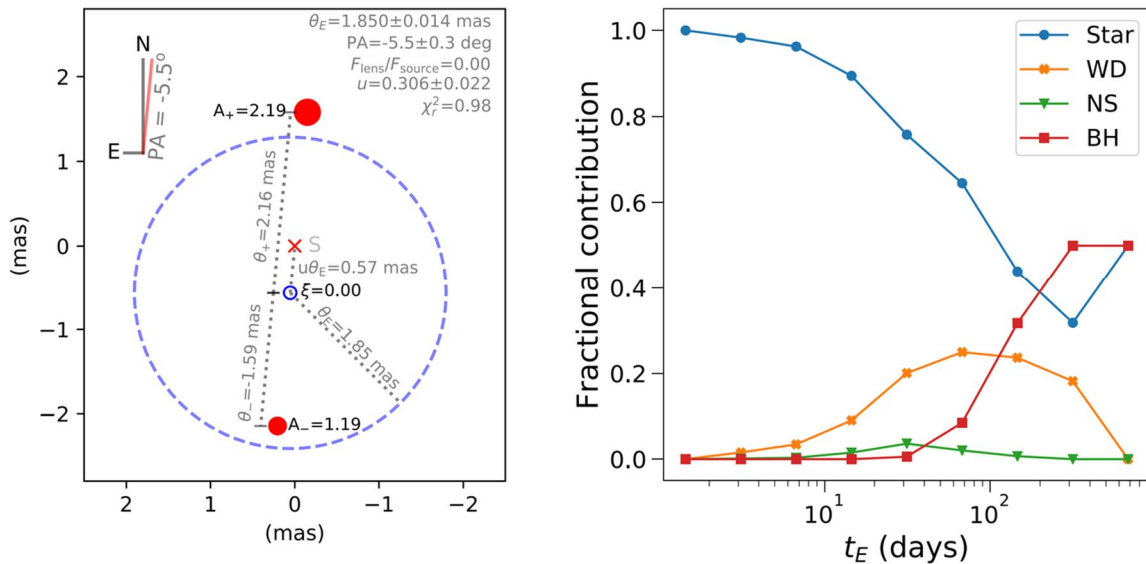
Figure 6: Left: the first resolution of a microlensed image by GRAVITY (Dong et al. 2019). Right: expected fractional contribution from stars, white dwarfs (WD), neutron stars (ND), and stellar black holes (BH) to WFIRST microlens events for different Einstein crossing times (Lam et al. 2019). For long crossing times > 300 days, 50 % of the events are expected to arise from black holes.

Not only dark objects are in need of mass measurements, but also stellar evolution models to tune their free parameters. Most of the mass estimates come from binary or multiple systems (see §3.5). However, there are important evolutionary differences between multiple systems and isolated stars (Sana & Evans 2011), and GRAVITY+ observations of micro-lenses will bring the crucial mass measurements of isolated objects. Finally, yet importantly, by a follow-up of microlensing events showing the signature of an exoplanet, GRAVITY+ will constrain how low-mass planet populations beyond the snow line (only accessible to microlensing) depend on their stellar host mass.

3.6 Massive Stars

Massive stars – together with massive black holes – drive feedback in galaxy evolution. With their fast stellar winds, huge mass-loss rates, intense ionizing radiation, and death in the form of supernova explosions (Zinnecker & Yorke 2007), these stars dominate the starburst phenomena, and they contribute a significant fraction of the feedback energy and momentum. Most massive stars live in multiple systems, the evolution of high mass stars strongly depends on multiplicity (Sana et al. 2012), and the multiplicity has a large impact on the formation of gravitational wave progenitors (Kruckow et al. 2018). Interferometry is a unique technique to study these massive binary systems (Figure 7).
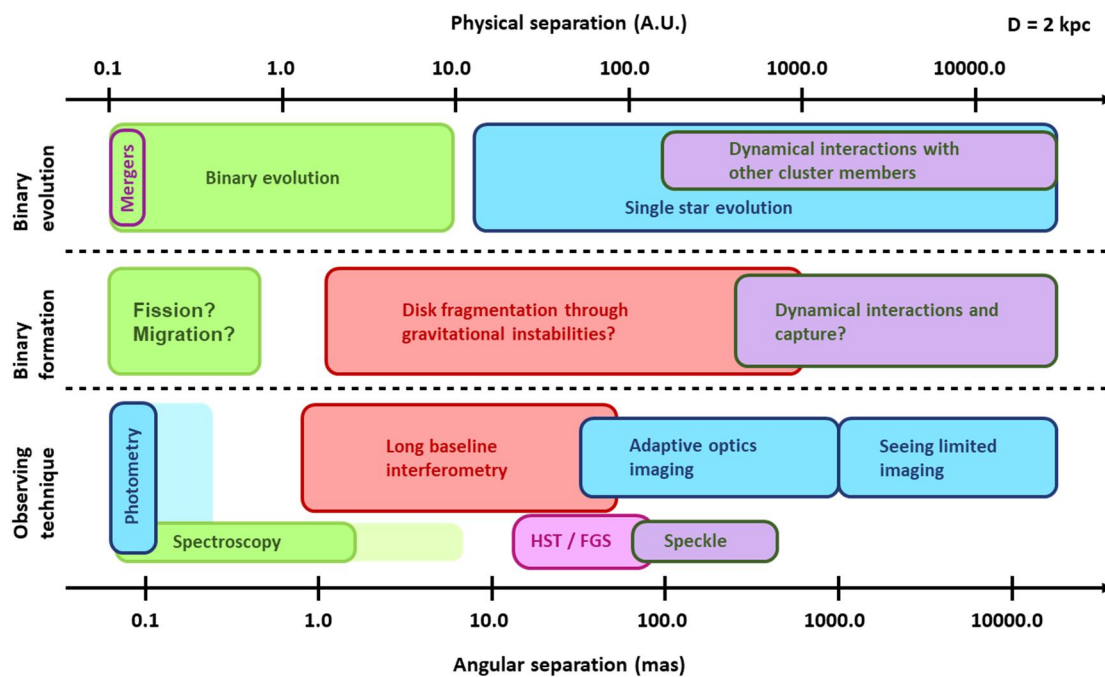
Figure 7: Schematic of the different techniques used to study multiplicity in massive stars (adapted from Sana 2017). Interferometry is the unique technique to bridge the gap between 'isolated' evolution and the regime of strongly linked evolution in close binaries.

GRAVITY+ will be able to resolve O/WR stars at the core of the most massive starburst clusters in the Galaxy and Magellanic Clouds, to:

- Characterize the upper end of the initial mass function (IMF), its universality, and the multiplicity (Schneider et al. 2018, Sana et al. 2013, GRAVITY collaboration et al. 2018e), thereby provide the basis for predicting GW progenitor rates and channels.
- Constrain the link between the Core Mass Function and the observed IMF. It is still under debate if the initial mass of the gas determines the final mass of the stars, or if the IMF is shaped from dynamical interactions in multiple systems (Offner et al. 2014).
- Provide high-angular resolution images of massive Young Stellar Object to clarify the role of core collapse (McKee & Tan 2002), competitive accretion (Bonnell et al. 2001), and disk fragmentation (Kratter & Lodato 2016).
- Measure the dynamical masses for the many systems detected by Gaia (at kilo-parsec distances, Gaia is sensitive to binaries whose radial velocities are undetectable).

3.7 Intermediate Mass Black Holes

The extrapolation of the relation between the mass of the central black hole M_{BH} and the bulge M_{Bulge} of galaxies to low masses argues for the existence of intermediate mass black holes (IMBH) at the cores of star clusters with $M_{BH} \approx 10^3 - 10^5 \, M_8$ (e.g., Portegies Zwart & McMillan 2002). Despite intensive searches, there are only a few tentative detections so far, e.g., 47 Tuc ($M_{BH} \approx \mathbf{2.3 \times 10^3} M_{\odot}$, Kiziltan et al. 2017) and ω Cen ($M_{BH} \approx \mathbf{0.9} - 4 \times \mathbf{10^4} M_{\odot}$, Noyola et al. 2008, but see also van der Marel & Anderson 2010). The existence and abundance of IMBHs however plays an important role in the evolution from stellar seed black holes to supermassive black holes.

Low number statistics of stars in the cluster core is the main limitation for detections based on velocity dispersion. This can be overcome with micro-arcsec astrometry. The circular velocity of a star at 0.1″ radius from a $10^4 \, M_\odot$ IMBH amounts to 2.6 mas/yr for a typical globular cluster distance of 8 kpc, and the acceleration of such a star in clusters such as ω Cen, M15 or 47 Tuc would be detectable in less than five years of GRAVITY+ observations.

ω Cen is by far the best candidate to search for an IMBH. With a total mass in excess of 4 million solar masses, it is the most massive and closest (D $\approx$ 4.8 kpc) cluster. An acceleration signal would be a factor > 10 larger than for any other cluster (Figure 8). The central 2″ of ω Cen contains $\approx$ 20 stars with K $\approx$ 13 - 15 mag, which could be efficiently monitored with the GRAVITY+ field-of-view, and whose motions could reveal the presence of an IMBH. A bright star (K $\approx$ 10.8 mag) is located at 7″ distance and is well suited for wide-field off-axis fringe tracking.
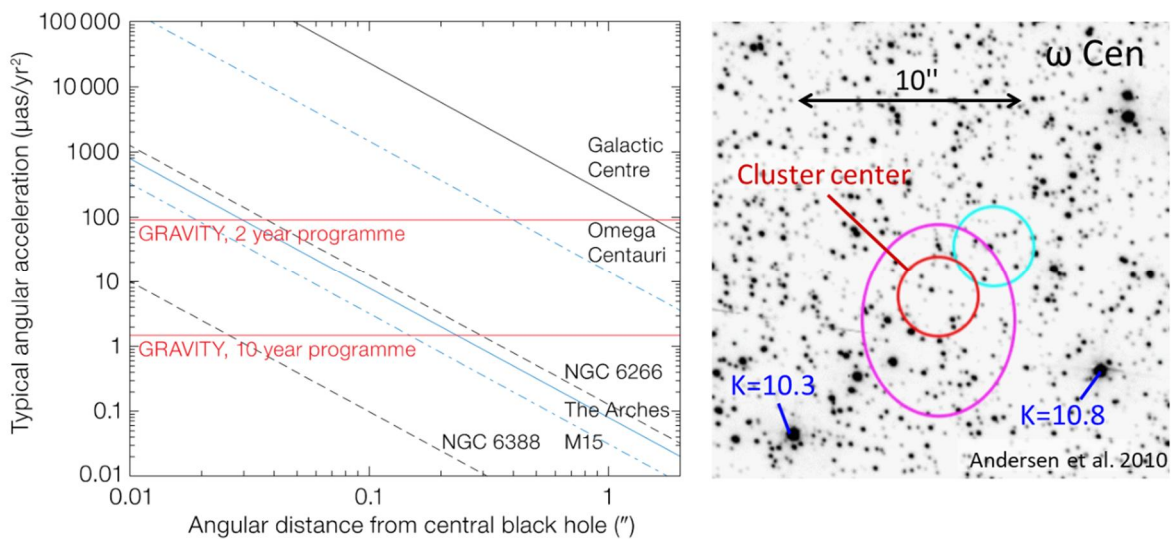
Figure 8. Left: Astrometric acceleration of a star orbiting putative intermediate mass black holes (IMBHs) in different clusters as function of angular separation from the IMBH. The red lines indicate the 5-sigma detection threshold for a 2-year and 10-year GRAVITY+ monitoring. Right: Central 20″ of ω Cen taken from Anderson et al. (2010). The red circle indicates the cluster center (based on HST number counts) and the $\approx$ 2″ uncertainty. The cyan circle denotes the 2MASS light center and the pink ellipse indicates the HST proper motion center.

4 Community Engagement

The coordinators of the six VLTI Expertise Centers from the European Interferometry Initiative are all members or supporters of GRAVITY+, demonstrating the strong connections between the community and the consortium.

The well-known tools used by the VLTI community for observation planning, data analysis, image reconstruction, standardized products (OIFITS, Duvert et al 2017), and integrated databases (available at http://www.jmmc.fr) will be upgraded to follow the new capabilities offered by GRAVITY+, in order to empower the VLTI users. Young and senior researchers will be trained to GRAVITY+ during the regular 'VLTI summer school' and 'VLTI community days', or by traveling to one of the VLTI Expertise Centers by means of the Fizeau exchange program.

Beyond its immediate powerful capabilities, GRAVITY+ will serve the ESO community by improving the VLTI infrastructure for existing instruments (MATISSE including GRA4MAT, PIONIER) and future visitor instruments (e.g., next generation fringe tracker, shorter wavelengths, nulling instruments).

Immediately at the start of the project, our team will organize an instrumentation-oriented workshop, bringing together GRAVITY+, ESO, and parties interested in the currently offered VLTI visitor focus. The goal will be to discuss the new VLTI capabilities provided by GRAVITY+ as well as their implications on existing and future visiting instruments, in order to preserve the coherence of VLTI and its instrument suite.

Later towards full GRAVITY+ science readiness, there will be a science-oriented workshop, addressing science capabilities, observation strategies, and data reduction techniques. With the involvement of the community, GRAVITY+ aims at extending the science made possible beyond the cases described in the present document.

5   Instrument Concept

5.1   Key Technical Requirements

The following table summarizes the top-level requirements for the GRAVITY+ upgrades, as driven by the three main pillars of the proposal: galactic center science, extragalactic and faint galactic science, and exoplanet / high-contrast science.

Table 1: Top-level requirements for GRAVITY+.

Science case	Science band	Strehl in science band	Guide star R-band magnitude	AO mode	Science K-band magnitude	Fringe trk. magnitude separation
Galactic Center	K-band	> 50%	14 (LGS)	LGS	up to 22	K = 10 at up to 30″
Extragalactic & Faint galactic	K-band	> 50%	18 (LGS) 10 (NGS)	LGS, NGS on/off-axis	up to 22	K = 13…15 at > 30″
Exoplanet & High Contrast	K-band	> 75%	10	NGS on-axis	up to 22	On-axis

NGS: natural guide star adaptive optics; LGS: laser guide star adaptive optics

5.2   GRAVITY+ Overview

GRAVITY+ combines upgrades and improvements of the GRAVITY instrument and the VLTI facility (Figure 9): the implementation of wide-field off-axis fringe tracking, new adaptive optics wavefront sensors and deformable mirrors on UT1,2,3,4, and the implementation of laser guide stars (LGS) for UT1,2,3.
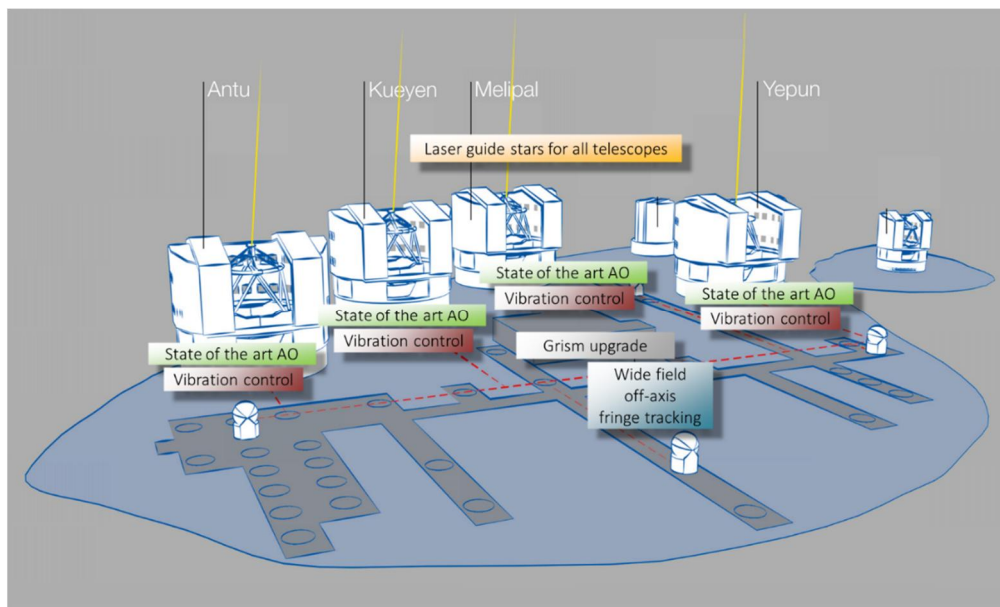

Figure 9: Upgrade of GRAVITY and the VLTI to GRAVITY+ for faint science, all sky, high contrast, milli-arcsecond interferometric imaging. The key elements are improved instrument throughput and vibration control, wide-field off-axis fringe tracking, state of the art adaptive optics, and laser guide stars for all telescopes.

5.2.1 Wavefront Sensors

The top-level requirements of the GRAVITY+ wavefront sensors (WFSs) are largely identical to the ones of ERIS, the adaptive optics assisted, multi-purpose imaging and spectroscopy instrument for the VLT (Davies et al. 2018). Consequently, our baseline is to replace the current, 15-year old, 60 element adaptive optics MACAO (Donaldson et al. 2000) sensors at the coudé focus (Figure 10) of each telescope with a modified version of the state of the art 40 x 40 elements ERIS sensors (Riccardi et al. 2018).

In this baseline design, the WFS is composed of two modules: the natural guide star (NGS) WFS and the laser guide star (LGS) WFS. Both are based on the standard ESO WFS Camera or an adaptation of the future ELT ALICE camera (both are CCD220).

- The NGS WFS is a high-order 40 x 40 Shack Hartmann (SH) sensor for NGS operation, and a low-order 4 x 4 SH array for measuring fast tip-tilt and low-order aberrations in LGS mode. The NGS WFS can patrol the full coudé focus field of view (FoV).
- The LGS WFS is a 40 x 40 SH sensor, with 6 x 6 pixel per sub-aperture and a FoV of 5″ to accommodate the elongated spots of the LGS. The LGS WFS is operated on-axis and does not require motorized stages to patrol the field.

The ERIS design will be adapted to the specific VLTI aspects, in particular to the coudé optics, the available volume, and the piston-free operation.

The baseline for the Real-Time-Controller is the Standard Platform for Adaptive optics Real Time Applications (SPARTA, Suárez Valles et al. 2012) upgrade / obsolescence program.

As part of the GRAVITY+ development, the team will explore possible improvements, e.g.,

- Use of a Pyramid sensor for even higher Strehl and better injection into single mode fibers. However, the reduced linearity of the Pyramid sensor may be problematic for correcting the non-common path aberrations down to the lab.
- Upgrade of the Real-Time-Controller with the goal to increase the correction bandwidth, and to increase synergies with next generation instruments, including ELT.

In both cases, any decision to depart from the baseline will be taken with great caution. The first objective of the GRAVITY+ consortium is to deliver the baseline within cost and schedule.

5.2.2 Deformable Mirrors

The current deformable mirrors (DMs) of the VLTI/UTs are the MACAO 60-actuator curvature mirrors. The number of actuators is barely enough for observations in the K-band under very good seeing, and dramatically fails in median seeing conditions or at shorter wavelengths. The scientific objectives of GRAVITY+ require replacing these 15-year old DMs with four new DMs with several hundred to a thousand actuators.
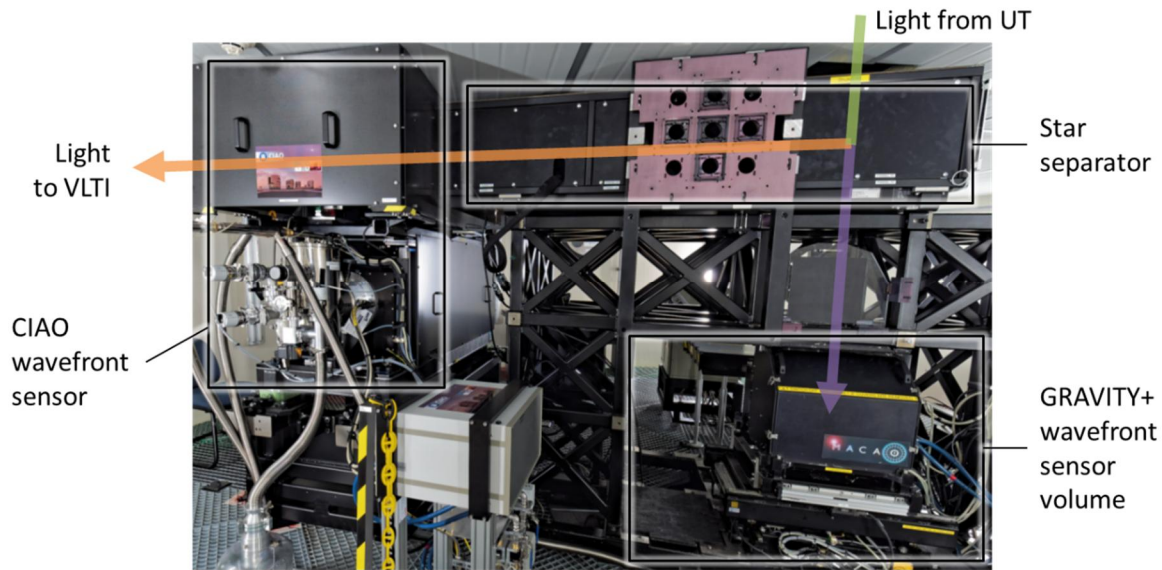
Figure 10: View of the coudé room below the UTs. The light from the sky and from the laser guide star enters the star separator (STS) module from top. The visible wavelengths (yellow) are transmitted toward the coudé focus behind the STS itself to feed the wavefront sensor (WFS). GRAVITY+ will upgrade the current WFS with a new state of the art WFS based on the ERIS design and will support both natural and laser guide stars.

The baseline is a 40 x 40 actuator, 2.5 mm pitch, DM from ALPAO, for which a rough order magnitude (ROM) offer is in hand (made available on request). The lead-time for the first DM is about 1 yr. The specifications of the DM are similar to the DM3228 recently produced by ALPAO and tested by LESIA (Vidal et al. 2019). Part of the non-recurrent cost of these DMs could be shared with ESO for the implementation of the mutually interesting 'high stability' option. Alternative and fallback options include:

- CILAS DMs with a 3.5 mm pitch (hence 29 x 29 actuators). CILAS is currently working on a ROM quotation (made available on request). CILAS DMs with this technology are already in use on 8m telescopes, and the specifications match our requirements.
- the development of a 5 mm pitch 24 x 24 actuator DM by ALPAO in the framework of a possible contract with Gemini Observatory. The time of development is estimated to be » 1 year.

The deformable mirrors will be mounted in a motorized tip/tilt stage with vertex point at the center of the mirror surface. These mounts are for quasi-static alignment only. If needed, the tip/tilt can be offloaded to the telescope secondary mirror with a closed-loop bandwidth of a few Hz.

5.2.3 Laser Guide Stars

The need for a bright guide star strongly limits the sky coverage of adaptive optics, and thereby interferometry. Especially, the low sky coverage at high galactic latitude prevents the efficient use of adaptive optics in extragalactic astronomy. Artificial laser guide stars (LGS) overcome this limitation (Davies & Kasper 2012).

24

Figure 11: GRAVITY+ will equip UT1,2,3 with a laser guide star. The baseline is a replica of the AOF LGS, or an adaption of the upcoming ELT LGS. Left: AOF launch telescope (ESO/G. Hüdepohl). Right: SodiumStar (Toptica Projects).

Following the first ESO laser guide stars PARSEC (Bonaccini Calia et al. 2006), the development of the compact and reliable Raman fiber laser technology (Bonaccini Calia et al. 2010), and the 4LGSF Adaptive Optics Facility (AOF, Arsenault et al. 2010), GRAVITY+ will now equip also UT1,2,3 with a side-launch LGS each. The GRAVITY+ baseline is to use the same LGS as used in the AOF 4LGSF, or an adaption of the ELT LGS. For UT4, GRAVITY+ will use one of the existing AOF LGS.

Figure 11 shows the main components of the proposed LGS for GRAVITY+, the launch telescope (left), and the laser unit (right). The technology is well developed and commercially available. Potential suppliers include Toptica for the laser units, and TNO, Toptica/Astelcon, KT Optics for the laser projection subunit including the launch telescope. Fixed price quotations and manufacturer cost estimates are available for all components. New laser developments (e.g., d'Orgeville et al. 2018) might allow for substantial cost reduction.

Our simulations, combining adaptive optics and fringe tracking performance, indicate that a single laser guide star results in a sky coverage only 15% below the sky coverage for two laser guide stars centered on the science object and tip-tilt / fringe tracking reference. To limit cost and complexity on both laser launch system and wavefront sensors, GRAVITY+ therefore adopts a single guide star as the baseline.

5.2.4 Dual-Field Infrastructure for Wide-Field Off-Axis Fringe Tracking

GRAVITY has demonstrated that interferometry can go as deep as K = 21 mag when using off-axis fringe tracking. But this capability is currently limited to extremely small sky coverage because the fringe tracking star must be within the 2″ field-of-view of VLTI. The solution to extend this patrol field to > 30″ already exists: the star separators (Delplancke et al. 2004) at the coudé focus of the UTs, the dual beam main delay lines, and the differential delay lines (DDLs, Pepe et al. 2008) in the VLTI laboratory. The baseline design for GRAVITY+ is to build on this available hardware. The six differential delay lines will be extended to eight to provide

a complete dual-field capability for four telescopes. The existing differential delay lines, initially designed for the PRIMA experiment (Delplancke 2008), need to be slightly modified to relay the dual-field VLTI pupil to the pupil location of the current instruments.

In addition, the dual-field beams arriving at the VLTI laboratory will be re-arranged into two close beams. This is the most cost effective and efficient way of upgrading GRAVITY, designed for off-axis but within a single field, to the wide-field off-axis dual-beam mode. This concept has already been demonstrated on-sky (see Figure 12). The corresponding periscopes will be modified for remote control.
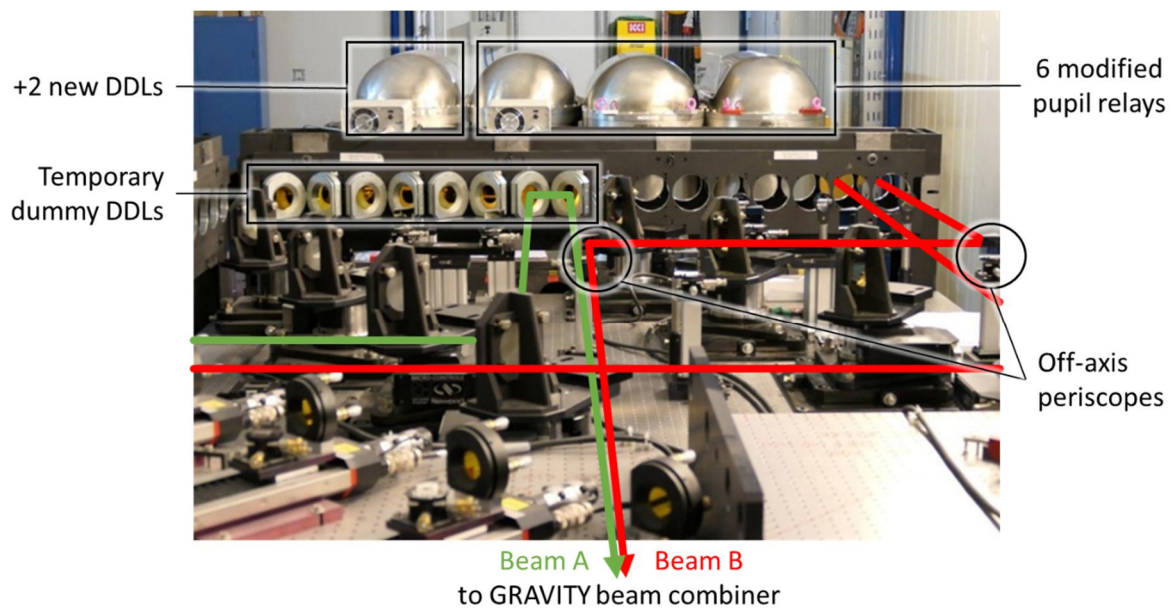

Figure 12: Modification of the dual-field infrastructure in the VLTI laboratory: The GRAVITY+ upgrade includes two new differential delay lines (DDLs), whose vacuum chamber is already existing, and the modification of the current six DDL for proper pupil relay. The picture also shows the off-axis periscopes and dummy DDLs used for the GRAVITY dual-beam off-axis demonstration. The periscopes will be modified for remote control, the dummy DDLs will be discarded to feed the new DDLs.

5.3 Technology Readiness

For the wavefront-sensor and lasers, our approach is to re-use or adapt existing systems and components. This approach guarantees reliable cost control and risk mitigation. The ERIS wavefront-sensor module will be installed in Paranal in 2020, demonstrating that our proposed wavefront-sensor concept is readily available. The AOF lasers have been in routine operation for several years, and deliver on expectation with an exquisite flux return.

The available offers demonstrate that the GRAVITY+ requirements on the DM can be fulfilled by ALPAO, and possibly CILAS, within a 1-year timeline for a first device. Our baseline is to initiate the process with ALPAO as a joint collaboration between GRAVITY+ and ESO in order to benefit from synergies with other ESO adaptive optics projects. There are no challenges in the design of the quasi-static mount of the DM.

Off-axis dual-field operation with GRAVITY at the VLTI has already been demonstrated with the ATs in November 2019, the demonstration with UTs is planned for March 2020. The required opto-mechanics are straightforward, and are largely a modification and duplication of existing motion control hardware.

5.4 Performance Breakdown

5.4.1 Performance Increase by Large Factors

GRAVITY has arguably transformed optical interferometry. However, its sensitivity is still far from the fundamental physical limits. The overall detective quantum efficiency is still somewhat below 1%, and substantially lower for faint objects, for which the quality of the adaptive optics wavefront correction is by far the dominant limitation. In addition, optical interferometry suffers from the fact that many perturbations enter exponentially. For example, a reduced Strehl exacerbates the impact of vibrations on the fringe tracker.

The philosophy behind the GRAVITY+ upgrades is to mitigate each of these limitations to deliver a combined increase in the overall performance by 4 – 5 magnitudes, a sky coverage comparable to current laser guide star adaptive optics, and a broadband off-axis limiting magnitude of up to K $\gg$ 22 mag.

- An upgrade of the GRAVITY spectrometers with (factor 2 – 3) higher throughput grisms was done in November 2019 in anticipation of GRAVITY+.
- Active and passive vibration control will reduce the fringe tracking residuals for the 8 m Unit Telescopes (factor 2).
- Implementation of laser guide stars and state of the art adaptive optics on all four UTs, which will improve Strehl ratios and coherent fluxes injected into the fibers (factor 4 – 10 for faint objects) and will increase the sky coverage dramatically.
- Higher Strehl ratios will also result in an increased stability of fringe detection (factor 2), which reduces the demand for the very best atmospheric conditions for faint interferometry.
- Revival of the differential delay lines will allow external fringe tracking on stars with a separation of > 30″ instead of 2″. This will not only provide the sky-coverage for extragalactic science, but also removes the need for splitting the light between fringe tracker and science channel (factor 2).

5.4.2 Strehl in NGS and LGS modes

The expected performances are readily available from the detailed analyses made for the ERIS instrument (*VLT-TRE-ERI-14403-3001-2.1)*. The main difference is the transmission to the coudé focus versus the Cassegrain focus. The six additional mirrors and the MACAO dichroic, which is optimized for broad-band reflectivity, lead to an additional light loss of up to one magnitude. The expected GRAVITY+ K-band Strehl ratio for bright objects is > 80 %, limiting magnitude for LGS operation with a K-band Strehl > 40 % is R = 18 mag (see Figure 13).

5.4.3 Sky Coverage for Off-axis Fringe Tracking

Figure 14 shows the expected sky coverage of GRAVITY+. Thanks to the dual-field infrastructure, the patrol field for the fringe tracking star will be > 30″. In median seeing conditions, this patrol field is entirely accessible because the iso-pistonic angle at Paranal in K-band is > 30″ (Elhalkouj et al 2008). The sky coverage is then defined as the probability for finding such a suitable fringe tracking star (K = 14 mag) for any given science object. Close to the Galactic plane, the sky coverage is almost 100 %. The probability to find a fringe tracking star is above 25 % for Galactic latitudes around 40°, and still around 10 % at the Galactic poles.
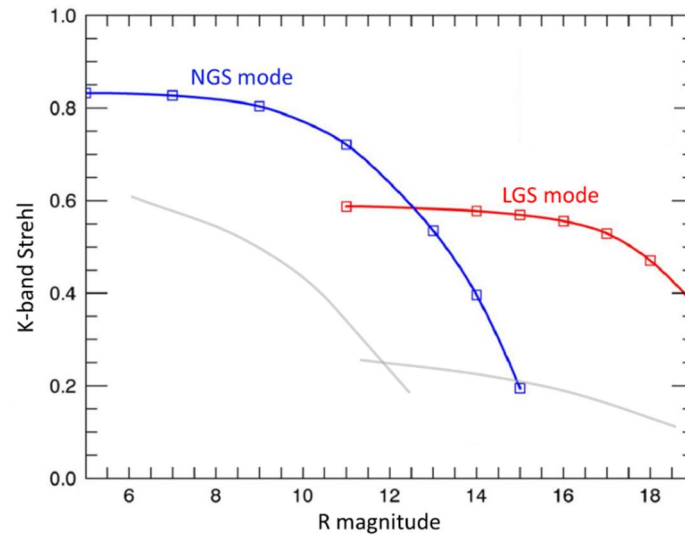
Figure 13: Predicted Strehl ratio of the GRAVITY+ adaptive optics for natural guide star (NGS, blue) and laser guide star (LGS, red) mode in K-band. For R magnitudes fainter » 12.5 mag, the LGS outperforms the NGS. The grey line indicates the Strehl ratio in J band. Adapted from simulations done for ERIS (VLT-TRE-ERI-14403-3001_2.1), taking into account 1 mag of additional throughput losses from the coudé optical train and the MACAO dichroic.
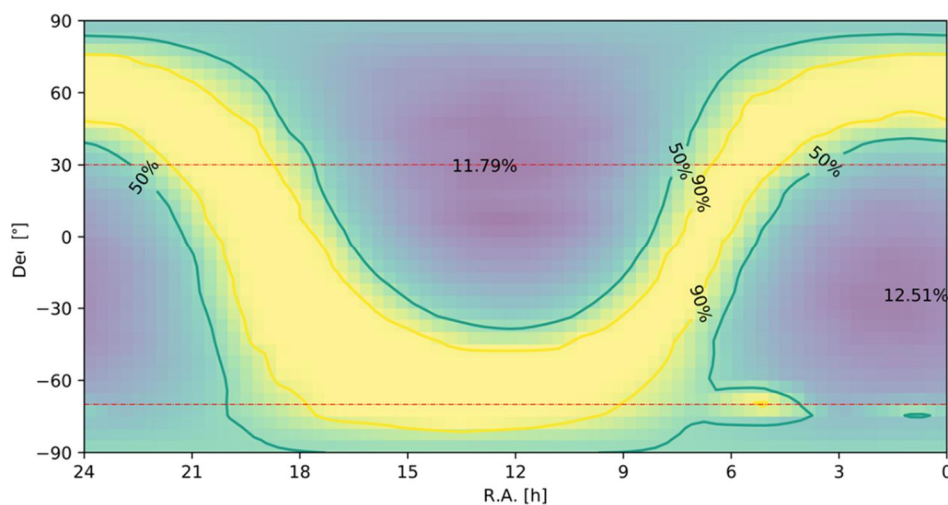
Figure 14. Sky coverage for finding a fringe tracking star with K < 14 mag at separations smaller than 30″, based on the 2MASS catalogue. Red lines encompass the part of sky accessible from Paranal (elevation > 35°).

6 Phased Implementation

The GRAVITY+ upgrades are implemented in three phases (Table 2, Figure 16), along and matching the phased approach and timeline in ESO's roadmap for the VLTI (Mérand 2018). The upgrades can be implemented incrementally, keeping the impact on operation to a minimum, and adding new, worldwide unique, science capabilities at every step.

Phase 1 encompasses the GRAVITY upgrade with higher throughput grisms, the implementation of the star-separator fed wide-field fringe tracking with GRAVITY, and continued reduction of vibrations and fringe tracker optimization. In Phase 2 the outdated MACAOs will be replaced with a state of the art adaptive optics wavefront sensors with high-order deformable mirrors, providing substantially improved limiting magnitude for extragalactic science and optimum performance for high contrast exoplanet observations. This advanced adaptive optics system will be already designed to support Phase 3, the laser guide stars on all telescopes, which will then fully open up the extragalactic sky.

All current VLTI instruments will benefit from the GRAVITY+ upgrades. The new adaptive optics and reduced vibrations will finally allow the PIONIER instrument to take advantage of the UT telescopes[2], and pushes the MATISSE instrument to unprecedented accuracy, therefore opening a new realm in high contrast interferometry.

Many GRAVITY+ upgrades are also critical pre-requisite for future visitor instruments. Examples are a next generation fringe tracker, shorter wavelength instruments, and nulling interferometers.

---

[2] Because of vibrations and insufficient AO correction in H-band, the sensitivity of PIONIER with UTs is about the same as with the ATs (see ESO/PIONIER call-for-proposal), while the nominal gain from the much larger UT light collecting area should be +3.2 mag.

7 Management Aspects

7.1 Consortium

The GRAVITY+ collaboration builds up and extends on the GRAVITY consortium and its institutional partners (Figure 15).

The GRAVITY consortium partner institutes MPE, ObsPM, IPAG, MPIA, UoC, and CENTRA remain full partners in GRAVITY+, in part with new CoIs: L. Kreidberg for MPIA, T. Paumard for ObsPM, J.-B. Le Bouquin for IPAG, Paulo Garcia for CENTRA. C. Straubmeier and F. Eisenhauer remain for UoC and MPE, respectively. The collaboration invites new partners to work together towards the GRAVITY+ goal of faint, all sky, high contrast interferometry with the VLTI. New partners with substantial financial or in-kind contribution would have full partnership including CoI representation (S. Hönig for UoS).

The GRAVITY+ collaboration further seeks synergy and collaboration with projects, institutes, and individuals for the science exploration, supplementary visitor instruments, and direct contributions. The currently associated partner projects are the visitor instrument suite ASGARD (D. Defrère (ULG), M. Ireland (ANU), S. Kraus (UoE), F. Martinache (Lab. Lagrange)), hierarchical fringe tracker (R. Petrov (Lab. Lagrange)), short wavelength beam combiner (S. Lacour (LESIA)), and direct contributions to vibration control (D. Defrère (ULG)). UoG will provide engineering support for the DDL upgrade and procurement (B. Chazelas).
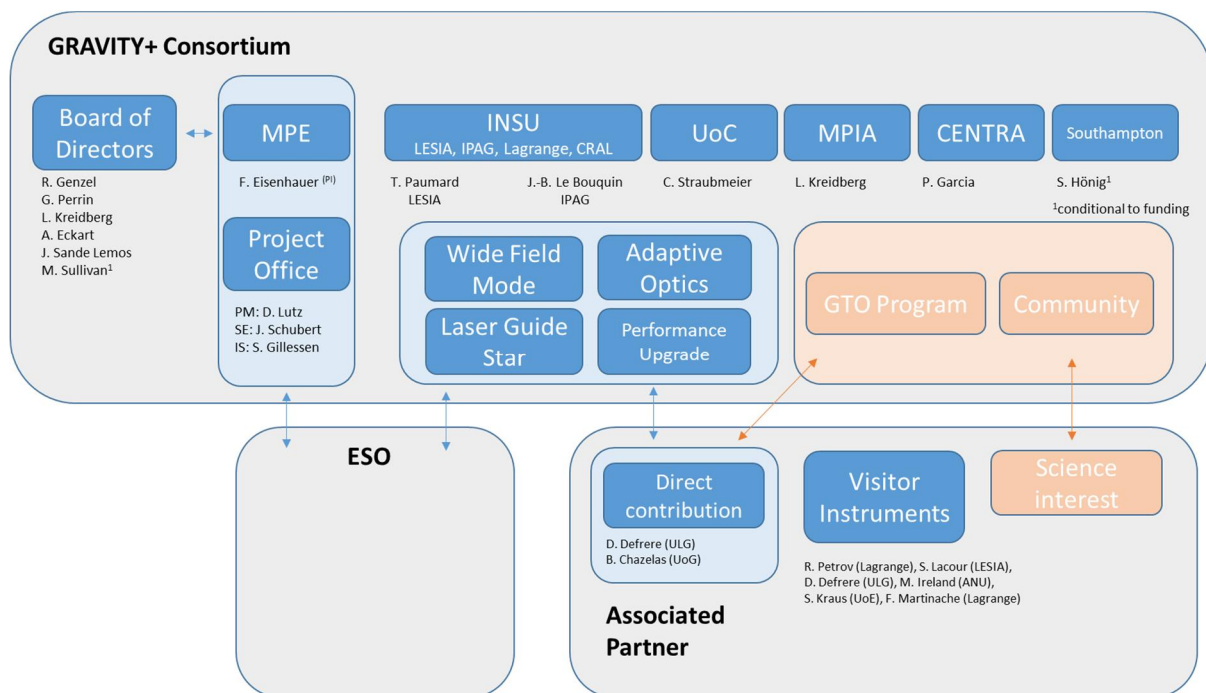

Figure 15: Structure of the GRAVITY+ consortium and the broader collaboration, which is including ESO and the associated partners. GRAVITY+ builds on and extends the successful GRAVITY consortium.

[Resource information has been removed from this copy]

7.2 Schedule

Figure 16 shows the schedule for GRAVITY+. Each upgrade can be implemented independently, and can start immediately. The phased implementation will minimize the impact on operation, and provide new science abilities at the end of each phase.
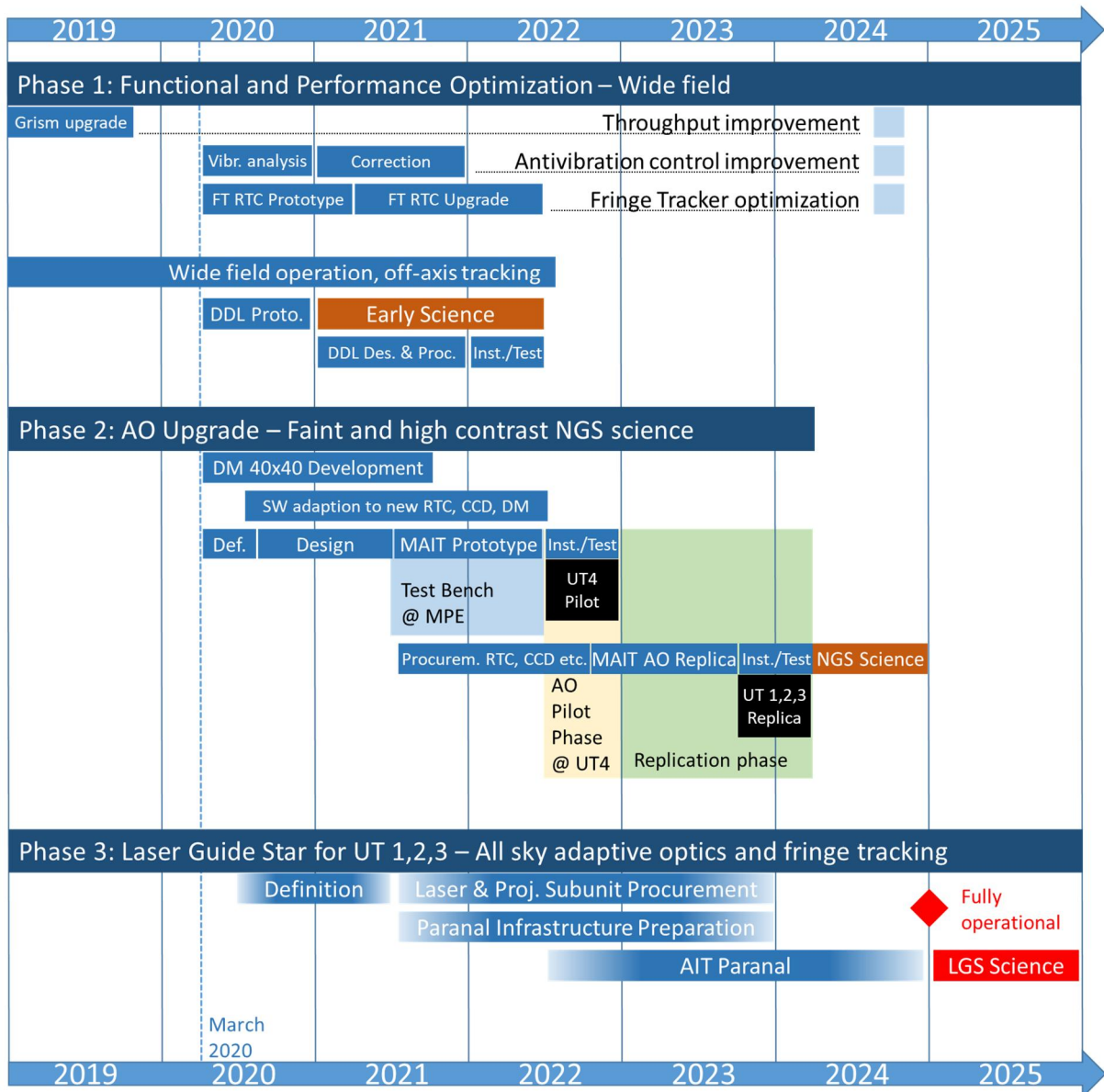
Figure 16: Schedule for the GRAVITY+ upgrades.

7.3 Risks

Risks of GRAVITY+ are reduced by the extensive reliance on the heritage of ERIS and the UT4 LGSF. In case of delayed development of the 40 x 40 actuator deformable mirrors, the fallback is the existing 25 x 25 technology, sufficient to serve the needs of all current VLTI instruments and for all laser guide star supported science. A later upgrade is straightforward.

8 References

Aird J., Coil A.L., Georgakakis A., et al. 2015, *The evolution of the X-ray luminosity functions of unabsorbed and absorbed AGNs out to z~5*, MNRAS, 451, 1892

Anderson J., van der Marel R.P. 2010, *New Limits on an Intermediate-Mass Black Hole in Omega Centauri. I. Hubble Space Telescope Photometry and Proper Motions*, ApJ, 710, 1032

Arsenault R., Madec P.-Y., Paufique J. et al. 2010, *Progress on the VLT Adaptive Optics Facility*, The Messenger, 142, 12

Bañados E., Venemans B.P., Decarli R. et al. 2016, *The Pan-STARRS1 Distant z > 5.6 Quasar Survey: More than 100 Quasars within the First Gyr of the Universe*, ApJS 227, 11

Baumgardt H., Amaro-Seoane P. & Schödel R. 2018, *The distribution of stars around the Milky Way's central black hole. III. Comparison with simulations,* A&A, 609, 28

Beckers J.M. 1993, *Adaptive Optics for Astronomy: Principles, Performance and Applications*, ARA&A, 31, 13

Begelman M.C., Blandford R.D., Rees M.J. 1980, *Massive black hole binaries in active galactic nuclei*, Nature, 287, 307

Bonaccini Calia D., Allaert E., Alvarez J.L. et al. 2006, *First light of the ESO Laser Guide Star Facility*, Proc. SPIE, 6272, 62721

Bonaccini Calia D., Feng Y., Hackenberg W. et al. 2010, *Laser Development for Sodium Laser Guide Stars at ESO*, The Messenger, 139, 12

Bonnell I.A., Bate M.R., Clarke C.J. et al. 2001, *Competitive accretion in embedded stellar clusters*, MNRAS, 323, 785

Bouvier J., Perraut K., Le Bouquin J.-B. et al. 2020, *Probing the magnetospheric accretion region of the young pre-transitional disk system DoAr 44 using VLTI/GRAVITY*, A&A, submitted

Bouvier J. & Appenzeller I. 2008, *Star-Disk Interaction in Young Stars*, IAU S243, Cambridge University Press

Bramich D.M. 2018, *Predicted microlensing events from analysis of Gaia Data Release 2*, A&A, 618, A44

Davies R., Kasper M. 2012, *Adaptive Optics for Astronomy*, ARA&A, 50, 305

Davies R., Esposito S., Schmid H.M. et al 2018, *ERIS: revitalising an adaptive optics instrument for the VLT*, Proc. SPIE, 10702, 1070209

Delplancke F., Nijenhuis J., de Manet H. et al. 2004, *Star separator system for the dual-field capability of the VLTI*, Proc. SPIE, 5491, 1528

Delplancke F. 2008, *The PRIMA facility phase-referenced imaging and micro-arcsecond astrometry*, NewAR, 52, 199

Donaldson R., Bonaccini D., Brynnel J. et al. 2000, *MACAO and its application for the VLT interferometer*, Proc. SPIE, 4007, 82

Dong S., Mérand A., Delplancke-Ströbele F. et al. 2019, *First Resolution of Microlensed Images*, ApJ, 871, 70

Du P., Zhang Z.-X., Wang K. et al. 2018, *Supermassive Black Holes with High Accretion Rates in Active Galactic Nuclei. IX. 10 New Observations of Reverberation Mapping and Shortened Hβ Lags*, ApJ, 856, 6

Duvert G., Young J., Hummel C. A. 2017, *OIFITS 2: the 2nd version of the data exchange standard for optical interferometry*, A&A 597, A8

d'Orgeville C., Fetzer G.J., Floyd S. et al. 2018, *Semiconductor guidestar laser for astronomy, space, and laser communications: prototype design and expected performance*, Proc. SPIE, 10703, 107030T

Einstein A. 1936, *Lens-Like Action of a Star by the Deviation of Light in the Gravitational Field,* Science, 84, 506

Eisenhauer F., Perrin G., Rabien S. et al. 2008, *GRAVITY: the AO-assisted, two-object beam combiner instrument for the VLTI*, in The Power of Optical/IR Interferometry: Recent Scientific Results and 2nd Generation, eds. A. Richichi, F. Delplancke, F. Paresce, & A. Chelli, 431

Elhalkouj T., Ziad A., Petrov R.G. et al. 2008, *First statistics of the isopistonic angle for long baseline interferometry*, A&A, 477, 337

Fernandes R.B., Mulders G.D, Pascucci I. et al. 2019, *Hints for a Turnover at the Snow Line in the Giant Planet Occurrence Rate*, ApJ, 874, 81

Finger G., Baker I., Alvarez D. et al. 2016, *Sub-electron read noise and millisecond full-frame readout with the near infrared eAPD array SAPHIRA*, Proc. SPIE, 9909, 990912

Genzel R., Eisenhauer F. & Gillessen, S. 2010, *The Galactic Center massive black hole and nuclear star cluster,* Rev. Mod. Phys., 82, 3121

GRAVITY Collaboration et al. 2017a, *First light for GRAVITY: Phase referencing optical interferometry for the Very Large Telescope Interferometer*, A&A, 602, 94

GRAVITY Collaboration et al. 2017b, *Accretion-ejection morphology of the microquasar SS 433 resolved at sub-au scale*, A&A, 602, L11

GRAVITY Collaboration et al. 2017c, *The wind and the magnetospheric accretion onto the T Tauri star S Coronae Australis at sub-au resolution*, A&A, 608, 78

GRAVITY Collaboration et al. 2018a, *Detection of the gravitational redshift in the orbit of the star S2 near the Galactic centre massive black hole*, A&A, 615, L15

GRAVITY Collaboration et al. 2018b, *Detection of orbital motions near the last stable circular orbit of the massive black hole SgrA**, A&A, 618, L10

GRAVITY Collaboration et al. 2018c, *GRAVITY chromatic imaging of η Car's core. Milliarcsecond resolution imaging of the wind-wind collision zone (Brγ, He I)*, A&A, 618, 125

GRAVITY Collaboration et al. 2018d, *Spatially resolved rotation of the broad-line region of a quasar at sub-parsec scale*, Nature, 563, 657

GRAVITY Collaboration et al. 2018e, *Multiple star systems in the Orion nebula*, A&A, 620, 116

GRAVITY Collaboration et al. 2019a, *Test of Einstein equivalence principle near the Galactic center supermassive black hole*, PhRvL, 122, 101102

GRAVITY Collaboration et al. 2019b, *First direct detection of an exoplanet by optical interferometry: Astrometry and K band spectroscopy of HR8799e*, A&A, 623, L11

GRAVITY Collaboration et al. 2019c, *A geometric distance measurement to the Galactic Center black hole with 0.33% accuracy*, A&A, 625, L10

GRAVITY Collaboration et al. 2019d, *The GRAVITY Young Stellar Object survey I. Probing the disks of Herbig Ae/Be stars in terrestrial orbits*, A&A, 632, A53

GRAVITY Collaboration et al. 2020a, *Detection of a parsec-scale dust ring in NGC1068*, A&A, 634, A1

GRAVITY Collaboration et al. 2020b, *Peering into the formation history of β Pictoris b with VLTI/GRAVITY long-baseline interferometry*, A&A, 633, 110

GRAVITY Collaboration et al. 2020c, *Detection of the Schwarzschild Precession in the Orbit of the Star S2 near the Galactic Centre Massive Black Hole,* in preparation

GRAVITY Collaboration et al. 2020d, *Resolving the magnetospheric accretion region in a Young Star*, Nature, submitted

Gualandris A. & Merritt D. 2009, *Perturbations of Intermediate-mass Black Holes on Stellar Orbits in the Galactic Center,* ApJ 705, 361

Jaffe W., Meisenheimer K., Röttgering H. J. A. et al. 2004, *The central dusty torus in the active nucleus of NGC 1068,* Nature, 429, 47

Jennison R.C. 1958, *A phase sensitive interferometer technique for the measurement of the Fourier transforms of spatial brightness distributions of small angular extent*, MNRAS, 118, 276

Johnson M.A., Betz A. & Townes C.H. 1974, *10-μm Heterodyne Stellar Interferometer*, PhRvL, 33, 1617

Jocou L., Perraut K., Moulin T. et al. 2014, *The beam combiners of Gravity VLTI instrument: concept, development, and performance in laboratory*, Proc. SPIE, 9146, 91461J

Kızıltan B., Baumgardt H., Loeb A. 2017, *An intermediate-mass black hole in the centre of the globular cluster 47 Tucanae*, Nature, 542, 203

Khabibullin I., Sazonov S., Sunyaev E. 2014, *SRG/eROSITA prospects for the detection of stellar tidal disruption flares*, MNRAS, 437, 327

Komossa S. 2015, *Tidal disruption of stars by supermassive black holes: Status of observations*, JHEAp 7, 148

Kopparapu R., Hébrard E., Belikov R. et al. 2018, *Exoplanet Classification and Yield Estimates for Direct Imaging Missions*, ApJ, 856, 122

Kratter K. & Lodato G. 2016, *Gravitational Instabilities in Circumstellar Disks*, ARA&A, 54, 271

Kreidberg L., Bean J.L., Désert J.M. et al. 2014, *A Precise Water Abundance Measurement for the Hot Jupiter WASP-43b*, ApJL, 793, 27

Kruckow M., Tauris T.M., Langer N. et al. 2018, *Progenitors of gravitational wave mergers: binary evolution with the stellar grid-based code COMBINE*, MNRAS, 481, 1908

Lacour S., Dembet R., Abuter, R. et al. 2019, *The GRAVITY fringe tracker*, A&A, 624, 99L

Lam C., Lu J., Hosek M.W. et al. 2020, *PopSyCLE: A New Population Synthesis Code for Compact Object Microlensing Events*, ApJL, 889, L31

Lazareff B., Berger J.-P., Kluska J. et al. 2017, *Structure of Herbig AeBe disks at the milliarcsecond scale. A statistical survey in the H band using PIONIER-VLTI*, A&A, 599, 85L

Leloudas G., Fraser M., Stone N.C. et al. 2016, *The superluminous transient ASASSN-15lh as a tidal disruption event from a Kerr black hole*, NatAs 1, 2

Léna P. 1979, *High spatial resolution by interferometry in the near infrared*, Journal of Optics, 10, 323. In French.

Léna P. & Merkle F. 1989, *The Interferometric Mode of the European Very Large Telescope*, Ap&SS, 160, 363

Li C., Ingersoll A., Bolton S. et al. 2020, *The water abundance in Jupiter's equatorial zone*, Nature Astronomy, https://doi.org/10.1038/s41550-020-1009-3

Lippa M., Gillessen S., Blind N. et al. 2016, *The metrology system of the VLTI instrument GRAVITY*, Proc. SPIE, 9907, 990722

Madau P., Dickinson M. 2014, *Cosmic Star-Formation History*, ARA&A, 52, 415

Madhusudhan N. 2019, *Exoplanetary Atmospheres: Key Insights, Challenges, and Prospects,* ARA&A, 57, 617

McKee C.F. & Tan J.C. 2002, *Massive star formation in 100,000 years from turbulent and pressurized molecular clouds*, Nature, 416, 59

Mérand A. 2018, *The VLTI roadmap*, The Messenger, 171, 14

Michelson A.A., & Pease F.G. 1921, *Measurement of the Diameter of α Orionis with the Interferometer*, ApJ, 53

Noyola E., Gebhardt K., Bergmann M. 2008, *Gemini and Hubble Space Telescope Evidence for an Intermediate-Mass Black Hole in ω Centauri*, ApJ, 676, 1008

Offner S.S.R., Clark P.C., Hennebelle P. et al. 2014, *The Origin and Universality of the Stellar Initial Mass Function*, Protostars and Planets VI, Henrik Beuther, Ralf S. Klessen, Cornelis P. Dullemond, and Thomas Henning (eds.), University of Arizona Press, Tucson, 914, 53

Pepe F., Queloz D., Henning Th. et al. 2008, *The ESPRI Project: differential delay lines for PRIMA*, Proc. SPIE, 7013, 70130P

Perraut K., Jocou L., Berger J. P. et al. 2018, *Single-mode waveguides for GRAVITY I. The cryogenic 4-telescope integrated optics beam combiner*, A&A, 614, 70

Pfuhl O., Haug M., Eisenhauer F. et al. 2014, *The fiber coupler and beam stabilization system of the GRAVITY interferometer*, Proc. SPIE, 9146, 914623

Pinte C., Price D.J., Ménard F., et al. 2020, *Nine Localized Deviations from Keplerian Rotation in the DSHARP Circumstellar Disks: Kinematic Evidence for Protoplanets Carving the Gaps*, ApJ, 890, L9

Portegies Zwart S.F., McMillan S.L. W. 2002, *The Runaway Growth of Intermediate-Mass Black Holes in Dense Star Clusters*, ApJ, 576, 899

Quirrenbach A. 2001, *Optical Interferometry*, ARA&A, 39, 353

Radigan J., Jayawardhana R., Lafrenière D. et al. 2012, *Large-amplitude Variations of an L/T Transition Brown Dwarf: Multi-wavelength Observations of Patchy, High-contrast Cloud Features*, ApJ, 105, 24

Regan J.A., Haehnelt M.G. 2009, *Pathways to massive black holes and compact star clusters in pre-galactic dark matter haloes with virial temperatures >~ 10000K*, MNRAS, 396, 343

Riccardi A., Esposito S., Agapito G. et al. 2018, *The ERIS adaptive optics system: from design to hardware*, Proc. SPIE, 10703, 1070303

Rosario D.J., McGurk R.C., Max C.E. et al. 2011, *Adaptive Optics Imaging of Quasi-stellar Objects with Double-peaked Narrow Lines: Are They Dual Active Galactic Nuclei?*, ApJ, 739, 44

Ryle M. & Hewish A. 1960, *The Synthesis of Large Radio Telescopes*, MNRAS, 120, 220

Sajadian S. & Poleski R. 2018, *Predictions for the Detection and Characterization of Galactic Disk Microlensing Events by LSST*, ApJ, 871, 205

Sana H., de Mink S. E., de Koter A. 2012, *Binary Interaction Dominates the Evolution of Massive Stars*, Science, 337, 444

Sana H., Evans C.J. 2011, *The multiplicity of massive stars*, IAU Symposium, 272, 474

Sana H., Le Bouquin J.-B., Mahy L. et al. 2013, *Three-dimensional orbits of the triple-O stellar system HD 150136*, Astronomy & Astrophysics, 553, A131

Sana H. 2017, *The multiplicity of massive stars: a 2016 view*, IAU Symposium, 329, 110

Schneider F.R.N., Sana H., Evans C.J. et al. 2018, *An excess of massive stars in the local 30 Doradus starburst*, Science, 359, 69

Shao M., Colavita M.M., Hines B.E. et al. 1988, *The Mark III stellar interferometer*, A&A, 193, 357

Scheithauer S., Brandner W., Deen C. et al. 2016, *CIAO: wavefront sensors for GRAVITY*, Proc. SPIE, 9909, 99092L

Solanes J.M., Perea J.D., Valenti-Rojas G. et al. 2019, *Intrinsic and observed dual AGN fractions from major mergers*, A&A, 624, A86

Songsheng Y.-Y., Wang J.-M., Li Y.-R. 2019, *Differential Interferometric Signatures of Close Binaries of Supermassive Black Holes in Active Galactic Nuclei*, 2019, ApJ, 881, 140

Straubmeier C., Yazici S., Wiest M., et al. 2014, *The GRAVITY spectrometers: optical design and first light*, Proc. SPIE, 9146, 914629

Suárez Valles M., Fedrigo E., Donaldson R. et al. 2012, *SPARTA for the VLT: status and plans*, Proc. SPIE, 8447, 84472Q

Tang J., Goto T., Ohyama Y. et al. 2019, *Rapid black hole growth at the dawn of the Universe: a super-Eddington quasar at z = 6.6*, MNRAS, 484, 2575

Thompson R., Moran J. & Swenson M. 2017, *Interferometry and Synthesis in Radio Astronomy*, Astronomy and Astrophysics Library, Springer International Publishing

van der Marel R. P., Anderson J. 2010, *New Limits on an Intermediate-Mass Black Hole in Omega Centauri. II. Dynamical Models*, ApJ, 710, 1063

van Velzen S., Farrar G.R., Gezari S. et al. 2011, *Optical Discovery of Probable Stellar Tidal Disruption Flares*, ApJ, 741, 73

Vasiliev E., Antonini F., Merrit D. 2015, *The Final-Parsec Problem in the Collisionless Limit*, ApJ, 810, 49

Vidal F., Raffard J., Gendron E. et al. 2019, *Tests and characterisations of the ALPAO 64×64 deformable mirror, the MICADO-MAORY SCAO AIT facility*, http://ao4elt6.copl.ulaval.ca/proceedings/401-PhKb-251.pdf

Waisberg I., Dexter J., Gillessen S. et al. 2018, *What stellar orbit is needed to measure the spin of the Galactic centre black hole from astrometric data?*, MNRAS 476, 3600

Waisberg I., Dexter J., Petrucci P.-O. et al. 2019, *Super-Keplerian equatorial outflows in SS 433. Centrifugal ejection of the circumbinary disk*, A&A, 623, A47

Wang J.-M., Qiu J., Du P., Ho L.C. 2014, *Self-shadowing Effects of Slim Accretion Disks in Active Galactic Nuclei: The Diverse Appearance of the Broad-line Region*, ApJ, 797, 65

Weigelt G., Hofmann K.-H., Kishimoto M. et al. 2012, *VLTI/AMBER observations of the Seyfert nucleus of NGC 3783*, A&A, 541, 9

Woillez J., Wizinowich P., Akeson R. et al. 2014, *First Faint Dual-field Off-axis Observations in Optical Long Baseline Interferometry*, ApJ, 783, 104

Woolf N. & Angel R. 1981, *MT-2*, in *Optical and Infrared telescopes for the 1980s*. Proceedings of the conference held 7-12 January, 1980 in Tucson, AZ. Edited by Adelaide Hewitt, p.1062

Zang W., Dong S., Gould A. at al. 2019, *Spitzer + VLTI-GRAVITY Measure the Lens Mass of a Nearby Microlensing Event*, arXiv:1912.00038v1

Zinnecker H. & Yorke H.W. 2007, *Toward Understanding Massive Star Formation*, ARA&A, 45, 481

Affiliations

[1] Max Planck Institute for Extraterrestrial Physics (MPE), Giessenbachstr.1, D-85748 Garching, Germany

[2] CENTRA – Centro de Astrofísica e Gravitação, IST, Universidade de Lisboa, 1049-001 Lisboa, Portugal

[3] Faculdade de Engenharia, Universidade do Porto, rua Dr. Roberto Frias, 4200-465 Porto, Portugal

[4] European Southern Observatory, Santiago 19, Casilla 19001, Chile

[5] Departments of Physics and Astronomy, Le Conte Hall, University of California, Berkeley, CA 94720, USA

[6] Department of Physics and Astronomy, University of Southampton,Southampton, UK

[7] Harvard-Smithsonian Center for Astrophysics, Harvard University, Cambridge, MA 02138, USA

[8] Max Planck Institute for Astronomy, Königstuhl 17, 69117, Heidelberg, Germany

[9] Université Grenoble Alpes, CNRS, IPAG, 38000 Grenoble, France

[10] LESIA, Observatoire de Paris, Université PSL, CNRS, Sorbonne Université, Université de Paris, 5 place Jules Janssen, F-92195 Meudon, France

[11] 1st Institute of Physics, University of Cologne, Zülpicher Straße 77, 50937 Cologne, Germany

[12] Universidade de Lisboa – Faculdade de Ciências, Campo Grande, 1749-016 Lisboa, Portugal

[13] Laboratoire Lagrange, UMR7293, Université de Nice Sophia-Antipolis, CNRS, Observatoire de la Côte d'Azur, Boulevard de l'Observatoire, 06304 Nice, Cedex 4, France

[14] Theoretical Physics Department, CERN 1 Esplanade des Particules, CH-1211 Geneva 23, Switzerland

[15] Space sciences, Technologies & Astrophysics Research (STAR) Institute, University of Liège, Liège, Belgium

[16] Sterrewacht Leiden, Leiden University, Postbus 9513, 2300, RA Leiden, The Netherlands

[17] Max Planck Institute for Radio Astronomy, Auf dem Hügel 69, 53121 Bonn, Germany

[18] Arcetri Astrophysical Observatory, Largo E. Fermi 5, 50125 Firence, Italy

[19] Universitäts-Sternwarte München, Scheinerstrasse 1, D-81679 München, Germany

[20] Research School of Astronomy & Astrophysics, Australian National University, Canberra, ACT 2611, Australia

[21] School of Physics, University of Exeter, Stocker Road, Exeter EX4 4QL, UK

[22] Laboratoire Lagrange, CNRS UMR 7293, UNS – Observatoire de la Côte d'Azur BP 4229, 06304 Nice Cedex 4, France

[23] School of Physics and Astronomy, EC Stoner Building, University of Leeds, Leeds LS2 9JT, UK

[24] ETH Zurich, Institute for Particle Physics and Astrophysics, Wolfgang-Pauli-Strasse 27, CH-8093 Zurich, Switzerland

[25] Instituto de Astronomía, Universidad Nacional Autónoma de México, Apdo. Postal 70264, Ciudad de México 04510, Mexico

[26] Univ. Lyon, Univ. Lyon 1, Ens de Lyon, CNRS, Ctr. de Recherche Astrophysique de Lyon (France)

[27] Centro de Astrobiología (CSIC-INTA), ESAC Campus, 28692 Villanueva de la Cañada, Madrid, Spain

[28] Unidad Mixta Internacional Franco-Chilena de Astronomía (CNRS, UMI 3386), Departamento de Astronomía, Universidad de Chile, Camino El Observatorio 1515, Las Condes, Santiago, Chile

[29] LUTH, Observatoire de Paris, PSL Research University, CNRS, Université Paris Diderot, 5 Place Jules Janssen, 92190 Meudon, France

[30] Institut d'Astrophysique de Paris, Sorbonne Université, CNRS, UMR 7095, 98 bis boulevard Arago, F-75014 Paris, France

[31] Department of Astronomy, University of Geneva, 51 Ch. des Maillettes, Sauverny CH-1290, Switzerland

[32] Dipartimento di Fisica dell'Universita and INFN, Torino, Italy

[33] Observatoire de Paris, LERMA, College de France, CNRS, PSL Univ., Sorbonne University, UPMC, Paris, France

[34] JILA and Department of Astrophysical and Planetary Sciences, University of Colorado Boulder, Boulder, CO 80309, USA

[35] Department of Physics, Kyoto Sangyo University, Kita-ku, Japan

[36] Dipartimento di Fisica e Astronomia, Università di Firenze, Via G. Sansone 1, I-50019 Sesto Fiorentino (Firenze), Italy

[37] Department of Astronomy, University of Michigan, West Hall, 1085 South University Avenue, Ann Arbor, MI 48109-1090, USA

[38] School of Physics and Astronomy, Tel Aviv University, Tel Aviv 69978, Israel

[39] Department of Astronomy, The Ohio State University, Columbus, OH, USA

[40] Center for Cosmology and AstroParticle Physics, The Ohio State University, Columbus, OH, USA

[41] Space Telescope Science Institute, Baltimore, MD, USA

[42] Institute of Astrophysics, KU Leuven, Celestijnlaan 200D, 3001 Leuven, Belgium